Performance Enhancement of Multi-tube Latent Thermal Energy Storage System: Optimization of Tube Shape, Placement and Shell Aspect Ratio

by

Syed Mohammed Tabish Haider

A thesis submitted in partial fulfillment for the
degree of Master of Science

in the

Faculty of Engineering
Department of Mechanical Engineering

2024

This postulation is dedicated to my parents, teachers and my wife, who are constantly a light for me in obscurity and their unflinching help, guided my unfocused words into Sound thoughts

CERTIFICATE OF APPROVAL

Performance Enhancement of Multi-tube Latent Thermal Energy Storage System: Optimization of Tube Shape, Placement and Shell Aspect Ratio

by

Syed Mohammed Tabish Haider

(MME221001)

THESIS EXAMINING COMMITTEE

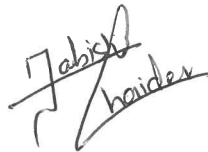| S. No.	Examiner	Name	Organization
(a)	External Examiner	Dr. Talha Irfan	IST, Islamabad
(b)	Internal Examiner	Dr. Muhammad Irfan	CUST, Islamabad
(c)	Supervisor	Dr. M. Mahabat Khan	CUST, Islamabad

Dr. M. Mahabat Khan
Thesis Supervisor
April, 2024

Dr. M. Mahabat Khan
Head
Dept. of Mechanical Engineering
April, 2024

Dr. Imtiaz Ahmad Taj
Dean
Faculty of Engineering
April, 2024

Author's Declaration

I, **Syed Mohammed Tabish Haider** hereby state that my MS thesis titled "**Performance Enhancement of Multi-tube Latent Thermal Energy Storage System: Optimization of Tube Shape, Placement and Shell Aspect Ratio**" is my own work and has not been submitted previously by me for taking any degree from Capital University of Science and Technology, Islamabad or anywhere else in the country/abroad.

At any time if my statement is found to be incorrect even after my graduation, the University has the right to withdraw my MS Degree.

(Syed Mohammed Tabish Haider)

Registration No: MME221001

Plagiarism Undertaking

I solemnly declare that research work presented in this thesis titled "**Performance Enhancement of Multi-tube Latent Thermal Energy Storage System: Optimization of Tube Shape, Placement and Shell Aspect Ratio**" is solely my research work with no significant contribution from any other person. Small contribution/help wherever taken has been duly acknowledged and that complete thesis has been written by me.

I understand the zero tolerance policy of the HEC and Capital University of Science and Technology towards plagiarism. Therefore, I as an author of the above titled thesis declare that no portion of my thesis has been plagiarized and any material used as reference is properly referred/cited.

I undertake that if I am found guilty of any formal plagiarism in the above titled thesis even after award of MS Degree, the University reserves the right to withdraw/revoke my MS degree and that HEC and the University have the right to publish my name on the HEC/University website on which names of students are placed who submitted plagiarized work.

(Syed Mohammed Tabish Haider)

Registration No: MME221001

Acknowledgement

In the Name of Allah, The Most Gracious, The Most Merciful. Praise be to God, the Cherisher and Sustainer of the worlds. All thanks to Almighty Allah, The Lord of all that exist, who bestowed me with His greatest blessing i.e. knowledge and Wisdom to accomplish my task successfully.

Thousands of salutations and benedictions to the Holy prophet Hazrat Muhammad (PBUH) the chosen-through by whom grace the sacred Quran was descended from the Most High. I am very thankful to Dr. Muhammad Mahabat Khan, a great teacher, mentor and supervisor who made a difference in all aspect of my life. I am indebted to Dr. Muhammad Mahabat Khan for his valuable guidance, encouragement and dedicated support that enabled me to complete my MS Degree Program.

I want to express my heartiest regards to my parents who always supported me morally, spiritually and prayed for my success.

(Syed Mohammed Tabish Haider)

Abstract

In the present study, performance enhancement of tubes-in-shell latent heat thermal energy storage unit (LHTESU), utilizing phase change material (PCM), was optimized by employing the Taguchi Method. It was identified that the energy storage effectiveness of LHTESU is influenced by critical design parameters, including the external geometry of the tubes (t_g = circular, Square, triangular), the aspect ratio of the rectangular shell (A_{r_s} = 4.23, 1, 0.48), and the location of the tubes from the bottom of the shell ($t_l = Z_B$, $0.5Z_B$, Z_{min}), where $Z_B = $ [(H-Z_{min})/4 -0.5D_h] depends on Height of the shell (H), external hydraulic diameter of the tube (D_h), and the minimum cutoff distance from bottom of the shell $Z_{min} = $ 5mm. The melting rate of the PCM was optimized using the Taguchi method by employing the L9 design table which reduced the number of simulation requirements from 27 to only 9 cases. The numerical computations were carried out by using the enthalpy-porosity model. The results from the Taguchi optimization show that the heat transfer fluid (HTF) carrying tubes of triangular shape arranged in a shell with an aspect ratio of A_{r_s}= 1 and tubes located at the bottommost configuration i.e., $t_l = Z_{min}$ maximize the melting perfor-mance of PCM. The optimized LHTESU configuration showed a 59% improvement in PCM melting rate compared to the base case, leading to an overall energy storage enhancement of 24%. For the optimum case, the temporal variation of energy performance parameters was also investigated at different HTF temperatures. The Nusslt number of the optimum case was observed to increase non-linearly as the HTF was varied from 318K to 368K resulting in a more than 60% increase in the Nusselt number.

Contents

List of Figures

List of Tables

Abbreviations

ANOVA	Analysis of Varience
Adj ss	Adjusted sums of squares
Adj ms	Adjusted mean squares
CFD	Computational Fluid Dynamics
Df	Degree of freedom
DOE	Design of Experiments
EPM	Enthalpy-porosity model
HTF	Heat Transfer Fluid
LF	Liquid Fraction
LHTESU	Latent Heat Thermal Energy Storage Unit
mins	minutes
MUSCL	Monotonic Upstream-centered Scheme for Conservation Laws
PCM	Phase Change Material
PISO	Pressure Implicit with Splitting of Operator
PRESTO	PREssure STaggering Option
SIMPLE	Semi-Implicit Method for Pressure Linked Equation
Seq ss	Sequential sums of squares
TES	Thermal Energy Storage

Symbols

Ar_s	Aspect ratio of shell
Q_{stored}	Amount of total energy stored by PCM
$\bar{Nu}$	Average nusselt number
S_B	Bouancy source term
Z_{cc}	Center to center distance between tubes, mm
Z_{min}	Clearance distance of HTF tubes from bottom
μ	Dynamic viscosity, $Pa.s$
d	Diameter of the tube, mm
E_r	Enhancement ratio
F_o	Fourier number
g	Gravity
T_{HTF}	Heat transfer fluid temperature, K
H	Height of the Shell, mm
D_h	Hydraulic diameter of tubes, mm
T_t	HTF tubes temperature, K
T_i	Initial temperature at tubes outer surface, K
ν	Kinematic viscosity, mm^2/s
T_l	Liquidious temperature, K
Δh	Latent heat of fusion
L	Latent heat capacity, kJ/kg
ϵ_o	Mean signal-to-noise ratio at optimal level
m_t	Melting time, mins
γ	Melting fraction percentage
S_{M_i}	Momentum source term

C_{Mushy} Mushy zone constant

T_{PCM} PCM temperature, K

Ra Rayleigh number

ρ_s Solidious density, kg/m^3

C_{PS} Specific heat capacity of PCM at solid state, $J/kg.K$

T_s Solidious temperature, K

Ste Stefan number

h Specific enthalpy, kJ/kg

C_{Pl} Specific heat capacity of PCM at liquid state

S/N Signal-to-noise ratio

β Thermal expansion coefficient, $1/K$

T_{os} Tube outer surface temperature, K

t Time, min

t_g Tube geometry

t_l Tube location

t_t Thickness of the tube, mm

k Thermal conductivity, $W/m.K$

Z_B Tubes distance from bottom of enclosure, mm

T Temperature, K

$a_{th,l}$ Thermal diffusivity

ϵ_l Total mean of signal-to-noise ratio

T_t Tube temperature, K

u_i Velocity of solid and liquid PCM, m/s

W Width of symmetric segment, mm

Chapter 1

Introduction

The sustainable growth of the contemporary world relies on the efficient utilization of energy resources. Fossil fuels currently constitute the predominant source of energy. Due to the depletion of current fossil fuel reserves and their harmful impact on the environment, there is a constant pursuit of energy sources that are efficient, environmentally friendly, and dependable. Renewable energy resources are indeed promising due to their environmental friendliness, however, they suffer from a lack of consistent supply. One potential resolution to this scenario is to employ energy storage systems, which include capturing and storing energy during periods of availability for later usage as needed. Various energy storage systems are utilized to store and recover different forms of energy. For instance, flywheels are used to store mechanical energy, batteries store electrochemical energy, biofuels store chemical energy, and thermal energy storages store thermal energy. Figure 1.1 illustrates the classification of several thermal energy storage methods. Thermal energy storage systems are economically effective, mitigate greenhouse gas emissions, and represent a promising advancement toward a low-carbon future. Additionally, they enhance the efficiency, credibility, and dependability of energy storage systems. Various LHTES systems are depicted in Figure 1.1. The effective thermal energy storage capabilities of LHTES systems have generated considerable interest in the past two decades. Various contemporary methods are employed to store thermal energy. Thermal energy storage involves energy storage at extremely low or high temperatures for subsequent use. The most straight-forward method

involves harnessing sunlight throughout the day to accumulate energy and use it during nighttime. A conventional charging-discharging process involves the act of replenishing the system with energy during periods of abundant availability, and subsequently utilizing that energy when required. This process is characterized by concurrency, with the system consistently doing the same actions repetitively. The LHTES system is a noteworthy technology that enables the long-term use of renewable energy systems.
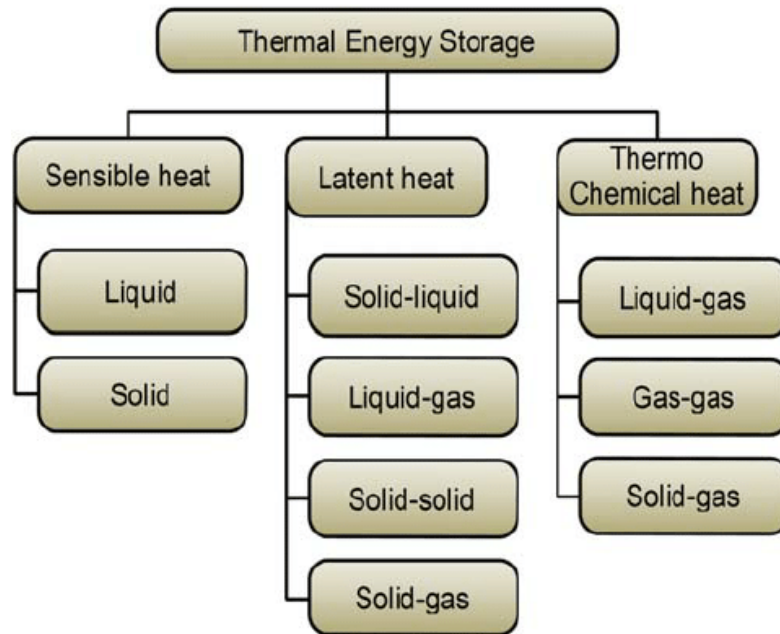
FIGURE 1.1: Classification of Thermal Energy Storage Systems [1].

1.1 Thermal Energy Storage

Thermal energy storage (TES) is a potential solution to address these difficulties by facilitating the effective capture, storage, and utilisation of surplus energy during times of low demand. This stored energy can then be used during peak demand hours or when there is insufficient generation of renewable energy. In their study, Nikolay et.al [2] examined various sustainable energy sources. There are primarily three types of TES systems, which are:

1. Sensible heat storage devices are designed to store heat by raising the temperature of a substance, such as water or rocks.

2. Latent heat storage systems include the storage of heat by inducing a phase change in a material, such as the conversion from solid to liquid or from liquid to gas.

3. Thermochemical storage systems utilize chemical reactions to collect and release heat, allowing for the storage of thermal energy.

1.1.1 Latent Heat Thermal Energy Systems

Latent heat thermal energy storage systems utilize the latent heat of PCM to store and release thermal energy. These systems are considered advanced technology. These systems are specifically engineered to effectively store and retrieve thermal energy for a range of purposes, such as heating, cooling, and power generation. The energy storage process in LHTES systems comprises three primary stages: charging, storage, and discharging.

1.1.1.1 Charging Process

Thermal energy is introduced into the system during the charging phase to cause a phase transition in the PCM, changing it from a solid to a liquid state. Typically, this is accomplished by subjecting the PCM to a heat source, such as solar radiation, waste heat generated by industrial operations, or surplus power derived from renewable sources. During the process of absorbing heat, phase change material experiences a phase transition, when it absorbs latent heat while keeping its temperature almost constant. The process of phase shift enables the PCM to efficiently store a significant quantity of energy as latent heat.

1.1.1.2 Storage

After the PCM has changed into a liquid, it keeps the thermal energy it has absorbed as latent heat. The system is then insulated to minimize thermal dissipation and sustain the phase of PCM as a liquid for a prolonged duration. This enables the system to efficiently retain thermal energy until it is required for heating, cooling, or other purposes.

1.1.1.3 Discharging Process

The LHTES system begins the discharging phase when there is a need for thermal energy. The PCM experiences a reverse phase transition from liquid to solid form when it is subjected to a colder environment via a heat exchanger. During the solidification process of the phase change material, it emits latent heat it has accumulated, which can then be transferred to a heat transfer fluid (such as air or water) that circulates within the system. Subsequently, this thermally charged fluid can be employed for diverse purposes such as heating spaces, warming water, or propelling a turbine to generate power. The system may consistently and reliably generate thermal energy, even in the absence of the primary heat source, due to the release of stored latent heat.

The LHTES system first stores sensible heat, but once the phase change temperature is reached, PCM temperature remains constant while the phase shift occurs and latent heat is stored. Solidification is the inverse process in which the PCM releases heat and undergoes a phase transition. Figure 1.2 illustrates the variation in the enthalpies of a storage medium during the processes of charging and discharging.
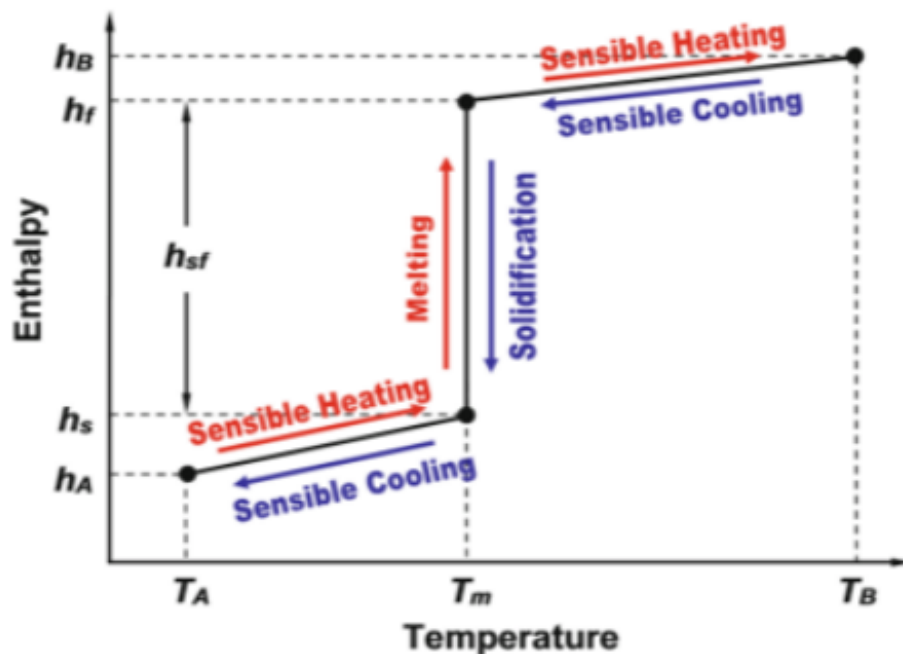
FIGURE 1.2: Enthalpy variation in phase change material during Heating and Cooling process [3]

1.1.2   Categories of Phase Transition

Phase change materials (PCMs) experience changes between solid, liquid, and gas phases in response to variations in temperature or pressure. The phase change materials undergo various sorts of phase transitions, including:

1.1.2.1   Melting (Solid to Liquid)

Melting is the process in which a substance changes from a solid state to a liquid one due to increased temperature beyond its specific melting point. During this phase transition, the phase change material (PCM) undergoes a process in which it absorbs thermal energy from its surroundings while keeping its temperature constant until the solid substance has completely transformed into a liquid state.

1.1.2.2   Solidification (Liquid to Solid)

Solidification refers to the process in which a phase change occurs from a liquid state to a solid state when the temperature of the phase change material (PCM) drops below its solidification point. During this phase transition, the phase change material (PCM) emits thermal energy to its surroundings while sustaining a consistent temperature until all of the liquid has fully solidified into a solid state.

1.1.2.3   Vaporization (Liquid to Gas)

Vaporization is the process in which a PCM transitions from a liquid state to a gaseous one due to an increase in temperature surpassing its boiling point. During this phase transition, the PCM undergoes a process of absorbing thermal energy from its surroundings in order to overcome inter molecular interactions and transition into a gaseous form.

1.1.2.4   Sublimation (Solid to Gas)

Sublimation is the phenomenon where a solid substance undergoes a direct transformation into a gaseous state without passing through the moderate liquid phase.

This happens when specific temperature and pressure parameters are met, enabling the solid to transition into a gas without undergoing liquefaction.

The preference for solid-liquid systems over others comes from the favorable properties of solid-to-liquid PCMs, which are highly suitable for storing thermal energy through latent heat. These systems offer efficient and dependable solutions for a range of industries, including buildings, solar energy systems, and HVAC systems. Additionally, solid-liquid phase change systems operate at lower pressures compared to alternative systems.[4]

The LHTES system unit consists of the following major components:

1.1.3 Phase Change Materials (PCM)

Phase change materials are materials that can store and release large amounts of thermal energy during phase shifts. They have the ability to undergo phase change, changing from a solid to a liquid or gas state, and vice versa, while either absorbing or releasing heat. Phase change materials (PCMs) find application in diverse fields such as building construction, electronics, transportation, and renewable energy systems for the purpose of storing and managing thermal energy.

1.1.4 Heat Transfer Fluid (HTF)

In a latent heat thermal energy storage system, the HTF serves as a medium for transferring heat between and within the phase change material throughout the process of charging or discharging. Phase change materials (PCMs) experience a transformation in their physical state, commonly transitioning from a solid to a liquid or vice versa. This process involves the absorption or release of a substantial quantity of latent heat, while the temperature remains relatively constant.

The selection of heat transfer fluid (HTF) is dependent upon several criteria, including the operational temperature range, compatibility with the phase change material (PCM) and system components, thermal stability, cost, and environmental effects. Common heat transfer fluids used in latent heat thermal energy storage systems include water, organic fluids like glycols, and molten salts such
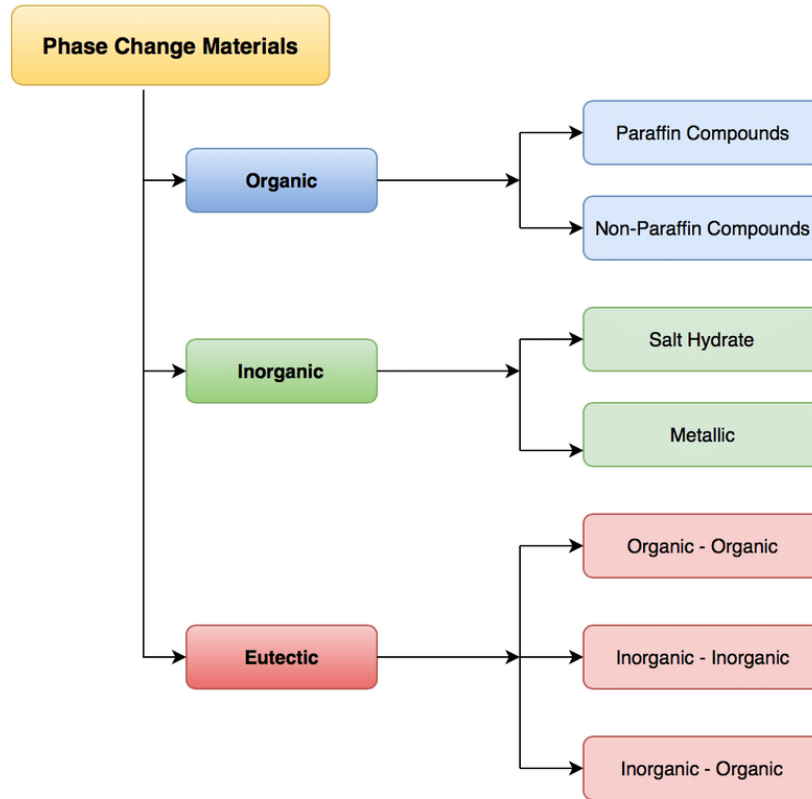
FIGURE 1.3: Types of Solid-Liquid phase change materials [5]

as sodium nitrate and potassium nitrate. Each option possesses unique benefits and constraints, and the choice is contingent upon the precise demands of the application.

1.1.5   Types of Solid-Liquid PCM

Solid-liquid PCMs are used in various applications for the purpose of storing thermal energy. This is because they have the ability to store and release energy as they change from a solid to a liquid state. Figure 1.3 illustrates many types of solid-liquid PCMs, which include:

1.1.5.1   Organic PCMs

Parafin Waxes: They consist of hydrocarbons characterized by extended alkane chains. Paraffin waxes are commonly employed as phase change materials (PCMs) because of their substantial latent heat of fusion, wide range of available melting

temperatures, and affordable price

Fatty Acids: Stearic acid and palmitic acid are examples of fatty acids, which are organic molecules that demonstrate phase transition characteristics. They provide a comparatively large amount of energy storage and exhibit excellent thermal stability.

1.1.5.2   Inorganic PCMs

Salt Hydrates: Water combines with inorganic salts to create hydrated salts, including sodium sulfate decahydrate, magnesium sulfate heptahydrate and calcium chloride hexahydrate. Salt hydrates possess a substantial amount of latent heat of fusion, making them well-suited for applications that need medium to high temperatures.

Metal Alloys: Some metal alloys exhibit solid-liquid phase change in specific temperature intervals, making them valuable as phase change materials (PCMs). Examples comprise indium, tin, and gallium alloys.

1.1.5.3   Eutectic PCMs

Binary Eutectic Mixtures: These are combinations of two substances that display a eutectic point, which is the state at which the mixture exhibits the lowest possible melting point. Binary eutectic mixtures provide accurate manipulation of the melting temperature but possess a significant capability for storing energy.

Ternary Eutectic Mixtures: Ternary eutectic mixtures, like binary eutectic mixtures, consist of three components and offer greater versatility in controlling the melting temperature and thermal characteristics.

1.1.6   Constraints of LHTES Systems

LHTES systems are often built to operate within certain temperature ranges determined by the phase change temperature of the selected PCM. Deviation from this range of temperatures can result in reduced efficiency or system malfunction.

The rate of heat transfer throughout the charging and discharging steps of LHTES systems may exhibit a slower pace in comparison to sensible heat storage systems. This constraint derives from the phase shift process, which demands additional energy input or extraction to alter the phase of the material.

Various techniques exist to enhance the transfer of heat. The goal of these methods is to enhance the thermal conductivity of phase change material in order to enhance heat transfer. This affects the phase change process and enhances overall performance. One method to increase thermal conductivity is by utilizing materials with high conductivity, such as metals, metallic oxide nanoparticles, and carbon compounds. Another method to improve the heat transfer of PCMs is by enhancing the natural convection of the liquid PCM. The commonly utilized LHTESUs include tube-in-shell, triplex-tube, and rectangular. Various tube geometries, such as rectangular, cylindrical, hexagonal, and circular, are frequently employed to enhance heat conductivity [6].

The study conducted by Sarbu and Dorca [7] investigated different methodologies to enhance heat transfer in thermal storage systems. The techniques used can be generally categorized into the following classifications:

1. Utilising high-conductive nanoparticles

2. Incorporating supplementary materials

3. Utilisation of encapsulation technique

4. Optimisation of tube positioning

5. Optimisation of shell geometry

6. Optimisation of tube geometry

7. Implementation of heat pipes

8. Implementation of cascaded storage

1.2 Integrating Thermal Energy Storage for Climate Control and Environmental Sustainability

Climate change is a significant and urgent problem that has wide-ranging impacts on ecosystems, the economy, and human welfare. To address climate change, it is necessary to implement creative strategies that decrease the release of greenhouse gases and improve the long-term viability of the environment. Thermal energy storage (TES) units offer promising avenues for addressing these challenges by optimizing energy usage, promoting renewable integration, and improving energy efficiency. In this context, exploring the role of TES in controlling climate change and enhancing environmental outcomes becomes imperative.

1.2.1 Energy Demand Reduction

TES systems enable the effective storage of excess power generated from renewable sources during times of reduced demand. Through the utilization of stored energy during periods of high demand, Thermal Energy Storage (TES) assists in decreasing the dependence on power generation derived from fossil fuels. Consequently, this action results in a reduction of greenhouse gas emissions and helps to decrease the consequences of climate change.

1.2.2 Optimizing Building Performance

Thermal energy storage (TES) systems, when incorporated into buildings, enhance the efficiency of heating, cooling, and ventilation systems. They achieve this by storing thermal energy while demand is low and using it to manage indoor temperatures when demand is high. By implementing this approach, energy consumption is reduced, running expenses are lowered, and emissions from heating and cooling equipment are decreased. As a result, indoor air quality and comfort are improved, while the environmental effect is reduced.

1.2.3   Improving Energy Efficiency

Thermal energy storage devices improve energy efficiency by absorbing excess thermal energy when available and releasing it when there is a high demand. This enhances the overall effectiveness of energy systems, decreases energy wastage, and decreases carbon emissions linked to energy generation, distribution, and usage.

1.2.4   Reducing the Urban Heat Island Effect

Thermal energy storage (TES) may reduce the urban heat island effect by accumulating surplus thermal energy produced during the day and utilizing it to cool buildings and outdoor areas at night. Thermal Energy Storage, increases urban comfort, air quality, and energy efficiency by lowering peak temperatures in metropolitan areas. This helps create a more sustainable urban environment

1.3   Scope and Objective of this Work

The current study attempts to fill this gap and propose multi-tube pattern shell and tube LHTES design for the melting enhancement of PCM. Rubitherm (RT-35) is used as PCM for the current study while water serves as HTF. Transient numerical simulations are performed to analyze the melting behavior of PCM in 2D planar configurations using commercial solver ANSYS Fluent. Numerical results are compared with the literature to validate the mathematical model used and the numerical solution strategy employed.The primary goal of this study is to enhance the melting performance of Phase change material (PCM) by optimizing the design parameters of the LHTES unit. Taguchi method is used as an optimization technique that proposes the optimum configuration of the shape of the tube, location of the tube, and aspect ratio of the shell. The performance of the new design configurations and the optimum case are examined by analyzing the melting fraction plots, average temperature distribution plots of PCM, specific heat storage and storage rates, and enhancement ratios. Furthermore, the impact of the heat transfer fluid (HTF) temperature on the performance is examined by

simulating optimal cases with varying Stefan numbers and observing the melting times and average Nusselt numbers.

1.4   Thesis Overview

Chapter 2 focuses on doing a literature survey specifically on phase change materials. In this chapter relevant work regarding the problem at hand will be discussed. A detailed literature review will be carried out about heat transfer augmentation techniques and methods involving PCMs.

Chapter 3 focuses on the numerical configuration of the simulation used to analyze the phase change process of the thermal energy storage unit. It contains a problem statement, analysis domain, and geometry. The content includes the meshing approach, boundary conditions, governing equations, and the Ansys Fluent setup for simulations.

Chapter 4 is related to the optimization of multi-tube LHTES units by using the Taguchi Method. In this chapter relevant work regarding Taguchi prediction and the percentage contribution of each parameter is discussed. The linear regression model is constructed and discussed in this chapter

Chapter 5 discusses the findings derived from this computational investigation. The result section is mostly broken into two pieces. The initial part comprises an examination of the distribution of melting fraction and temperature, comparisons of energy storage, and ratios of melting enhancement. The second section examines the impacts of altering the temperature of the heat transfer fluid (HTF) in the optimal configuration case. Correlations are suggested for the most optimum configurations, which are determined by non-dimensional Stefan, Nusselt, Fourier, and Rayleigh numbers.

Chapter 6 presents the conclusion of this research. This chapter also includes future recommendations related to the subject of the study discussed in this research.

Chapter 2

Literature Review

The long-term growth of modern civilization depends upon the efficient utilization of energy resources. The primary source of modern energy derives from fossil fuels. The search of sustainable, effective, and dependable energy sources is driven by the depletion of current fossil fuel reserves and their adverse ecological consequences. Renewable energy sources are widely seen as promising options due to their environmentally beneficial nature; yet, their constant supply remains a significant limitation. One potential approach to address this situation involves the implementation of energy storage systems, which involve the storing of energy during periods of availability for future utilization as needed. Various energy storage systems are utilized to store and recover diverse forms of energy. Examples of energy storage technologies include flywheels for mechanical energy storage, batteries for electrochemical energy storage, biofuels for chemical energy storage, and thermal energy storage (TES) for thermal energy storage, etc. Considering the current worldwide scenario that includes an ever increasing need for energy, it is evident that relying entirely on fossil fuels would inevitably lead to an upcoming energy crisis, especially among developing countries. The energy demand surpasses the available supplies. It is essential to acknowledge that there is a need for a dependable resolution to address the challenges related to energy. It is generally accepted that solar radiation is commonly regarded as a highly possible energy source in many countries. The global community has witnessed a notable shift in opinions regarding thermal energy storage systems over the past decade.The growing

popularity of thermal energy storage devices can be associated to their economic feasibility and efficiency. They are capable of offering a greater capacity for energy storage in comparison to other counterparts. The increasing significance of PCM is due to their environmentally friendly properties. This technology utilizes phase change material (PCM) as an energy source and offers an optimal option for meeting energy demands. The TES systems offer cost efficiency, as well as the potential to significantly reduce greenhouse gas emissions, providing an optimistic advancement towards a future that includes reduced carbon emissions. Energy storage devices also enhance performance, authenticity, and dependability.

The availability of renewable thermal energy is extensive in many geographical areas worldwide, predominantly in the form of solar radiation.Efficient energy storage can be achieved through two distinct methods: sensible energy storage, which involves raising the temperature of the system or material, and latent energy storage, which includes shifting the phase of the PCM. Thermal energy storage has the potential to address numerous serious issues; yet, continuous enhancements are necessary to meet the growing demands of an increasing population.Various enhancements can be achieved by the utilization of various materials, thermal energy storage systems, parameters, configurations, and numerous other variables.

There are several advantages related to LHTES devices as compared to their counterparts [8]. The LHTES system has a higher energy density, leading to less demand for material weight and volume to store an equivalent quantity of energy. The energy storage takes place at a consistent temperature, precisely at the phase change temperature of the phase change material. There are a broad range of PCMs that possess a wide range of melting temperatures. In order to be suitable for a specific application, it is necessary that the phase change material undergoes the process of melting within the specified temperature range. Researchers have primarily focused on the application domains ranging from 0 to 65 °C.These industries involves residential heating and cooling [9, 10], electronic equipment cooling [11, 12], solar energy thermal storage, and refrigeration applications [13, 14], etc. Researchers are now examining several designs of the LHTES systems under the specified design criteria. The many categories of systems include cylindrical shell
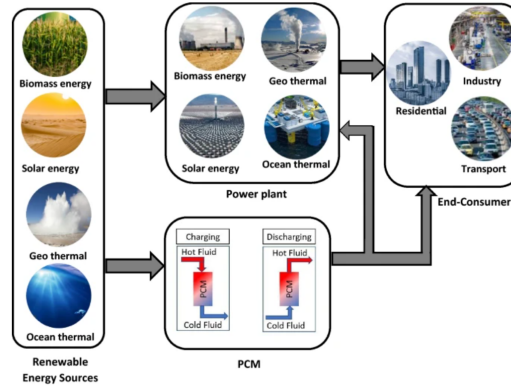
FIGURE 2.1: Applications of latent heat thermal storage system. [15]

and tube components, which can be arranged in either a horizontal or vertical orientation, alongside rectangular or slab-type systems. The horizontal orientation of the concentric shell and tube heat exchanger is widely regarded as the most straightforward design, primarily because it exhibits higher thermal performance in comparison to the vertical design [16].The PCM is placed between the outer shell and the inner tube. The inner tube is passed by the HTF, leading to the melting of the phase change material , a process commonly called as charging.The vertical displacement of the molten PCM is due to the phenomenon of buoyancy, which induces convective currents and speed up the PCM melting at the initial stages. Although the lower portion of the container undergoes a prolonged melting process for phase change material as a result of the significantly insufficient thermal conductivity demonstrated by the majority of PCMs. This particular characteristic provides an obvious disadvantage. The effectiveness of latent heat thermal energy storage systems is an issue due to the long period of time needed for the complete melting of the PCM within the system.

2.1 Various Techniques to Enhance LHTES System Efficiency

Numerous methodologies have been proposed and experimented with research in order address this issue, with the objective of enhancing the heat transfer rate between HTF tubes and the PCM throughout the charging and discharging processes.These methods cover a range of approaches, such as placing HTF tubes

at different locations inside the enclosure [17], utilizing different HTF tubes geometeries [18], utilizing different shell geometry [19], utilizing diverse fin shapes [8, 20, 21], incorporating nanoparticles [22–24] , employing metal foams [25, 26], incorporating highly conductive particles within the phase change material (PCM) [**?**], utilizing multi-tube shell and tube heat exchangers [27, 28], and implementing micro-encapsulation of the phase change material [29–31]. Rathod et al. [32] Performed an experimental study on the vertical orientation of an LHTESU having longitudinal fins and utilizing Stearic Acid as the PCM. The presence of longitudinal fins reduces the charging time of PCM by more than 43.6%. Abhat et al. [33] conducted an empirical investigation to assess the efficiency of a shell-and-tube heat exchanger using three distinct PCMs: paraffin, fatty acid, and salt hydrate. These PCMs have melting points ranging from 20 to 80 degrees Celsius. The PCM container utilized an annular shape heat exchanger. The results demonstrate a significant impact of temperature cycling and natural convection on both the charging and discharging efficiency of the storage materials. Liang et al. [34] investigated a thermal energy storage unit that utilizes a radial finned shell and tube configuration as shown in Figure 2.2. This research aims to determine the optimal configuration of radial fins to increase the rate of PCM melting in a vertical latent heat thermal energy storage (LHTES) unit. The numerical simulation initially studied the impact of adding aluminum fins, which have significantly better heat conductivity than PCM, on the melting process. The total charging time of the radial finned latent heat thermal energy storage system is reduced by 44.0% as compared to the latent heat thermal energy storage system unit without fins. Next, they examine the combined impact of fin elevation and angle on thermal performance. In this investigation, a non-dimensional fin height of 0.642 has been proposed. The experimental investigation conducted by Al Hinti [9] examined the use of water as a PCM within a solar water heating system. Through the utilization of water as PCM, the water had a temperature that was 30 degrees Celsius higher compared to the surrounding ambient temperature. Yosr Allouche [10] conducted a study on an developed solar-driven ejector-based air conditioning system utilizing phase change material. This study shows that phase change material has the potential to be utilized not just for heating applications but also for cooling purposes, especially within the air conditioning industry. The research
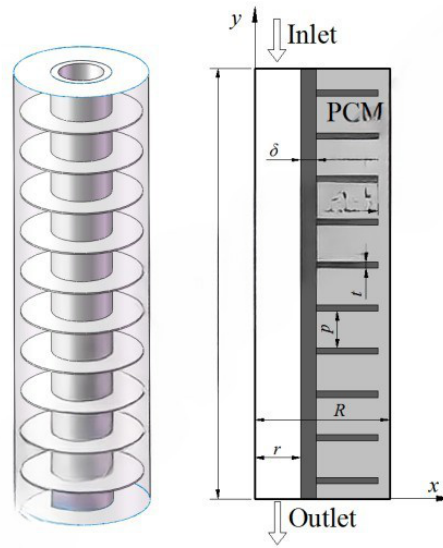
FIGURE 2.2: Schematic representation of radial finned shell and tube latent heat thermal storage system. (Reprinted from Liang et al. [34])

conducted by Mahdi et al. [35] used static structures and nanostructured materials to improve thermal performance. The hybrid method was also studied. It was found that heat transfer tubes with fins and metal foam work well together to improve. Each method has its challenges, but when considering free convection and heat transfer in design, none is better. Similarly, the impacts of different PCM mixtures contained within air channels, acting as a TES component for the air-cooling system of a standard building located in Nagoya, Japan, were investigated by Yamaha et al. [36]. The research revealed that a PCM with a mass of 5.4kg per square meter is enough to maintain a standard ambient thermal state for 180 minutes. Dolado et al. [37] studied the main performance control parameters of a long-term high-temperature energy storage system. The outcomes indicated that the operational efficiency of the system could be controlled through the arrangement of the PCM level, the number of ventilation ducts for fresh air, and the fluid rate of the HTF. Similarly, the study conducted by Waqas and Kumar [38] utilized solar energy to facilitate the heating of a building utilizing PCM as the energy storage material. The optimal system's performance is based upon the design of the working fluids flow rate, phase change material volume, and fusion heat, which are critical factors. Huang et al. [39] optimized the charging process of a horizontal LHTES unit by using Taguchi method. The study examined the impact of inner tube eccentricity, fin deflection angle, and fin width on the melting

enhancement of the PCM. It was noted that among the all the design parameters, the eccentricity of the HTF tubes significantly influenced the charging rate of the PCM. The results showed that, in comparison to the concentric four-fin LHSU, the optimal configuration with the heat transfer tube positioned at the bottommost location and a distribution of crown-shaped three-fin design exhibited a reduction in charging time by 64.1% and enhance the overall heat storage rate by 168.4%.

Shen et al. [40] investigated the geometric optimization of a LHTES unit using an analytical method with RT27 as the PCM to determine the ideal shape that gives the best heat transfer property. The most effective shape factor, according to the results, is about 0.15. Huang et al. [41] performed an analysis of the melting process in containers with rectangular, elongated, and curved shapes. They based their analysis on the concept of co-factor design, which is defined as the vector product of velocity magnitude and temperature gradient. This method enhances the rate of natural convection of liquid PCM which induces the buoyancy-dominant melting of the PCM and thus melts the PCM located far from the heating surface. Designed by these principles and the Co-factor method, an optimum phase change material container is suggested. This container has an elongated and curved shape, and it is compared to a rectangular container. It was observed the charging rate of the phase change material in the enhanced container can be decreased by over 20%. Khedher et al. [42] investigated the PCM melting of a vertical LHSU by altering the shape of the container that holds the PCM. The design modifications were intro-duced by inserting framed smooth, zigzag, forward, and reverse arced structures within the PCM container. The study examined and compared framed structures with unframed enclosures. The results indicated that a reverser arc structure re-duced the melting time by almost 43% while zigzag structure acceler-ated the melt-ing rate by 29% as compared to smooth structure. Francesco et al [**?**] examined the thermal efficiency of two different configurations of LHTES as illustrated in Figure 2.3. The numerical model combines the equations for mass, momentum, and energy of the PCM, together with an Enthalpy-Porosity model for phase change and a Boussinesq approach for the buoyancy force. The objec-tive of this study has been to improve heat transmission efficiency in LHTES by enhancing convection through adjustments to the geometry of the enclosure. This

study examines the impact of convective motion on the total melting time by considering two different geometries. In the first scenario, two cylinders are positioned one inside the other, with their axes aligned in the vertical direction. In the second case, the authors suggest using a straightforward cylindrical shape filled with the phase change material. The cylinder is positioned vertically with its axis aligned accordingly. The investigation demonstrates a significant difference in the thermal efficiency of the two proposed systems. The external heating configuration significantly improves the convective motion within the PCM, which leads to an increase heat transfer compared to the typical "shell-and-tube" configuration. The total duration of the phase transition process for the PCM when subjected to external heating is decreased by approximately 50%.
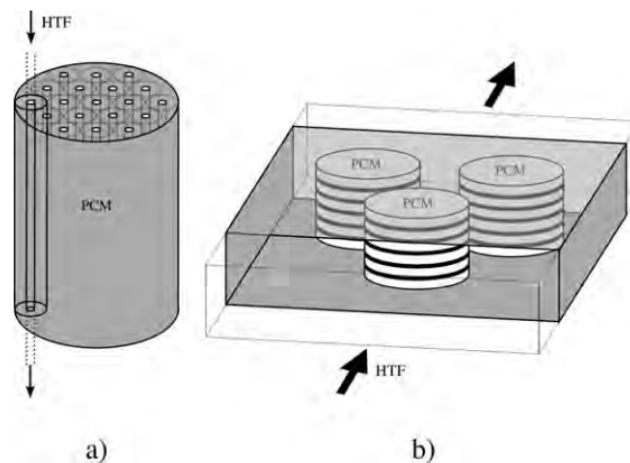
FIGURE 2.3: Schematic representation of storage enclosure a) shell and tube, Case 1 configuration. b) Case 2, cross flow between cylindrical PCM moduales and HTF. (Reprinted from Francesco et al. [43])

Mishra et al. [44] examine the melting process and heat transfer properties of a circular cylinder that is heated at a constant temperature. The cylinder is put inside twelve enclosures of varying shapes, which are filled with lauric acid, a phase change material. The research is conducted at two distinct temperatures on the surface of the heated cylinder, specifically 333.15 K and 343.15 K. The duration needed to achieve complete melting is primarily influenced by the quantity of PCM located above the heated cylinder, as well the interactions within the thermal boundary layers that lie at the adiabatic wall and the surface of the cylinder. The study presents comprehensive results on streamlines, rate of melting,

and temperature contours, to illustrate how the design of the enclosure affects the efficiency of the TES unit. The results indicate that out of every design examined, the inverted semi-circular enclosure leads to the most rapid melting and reduces the complete charging time four times.

Bai et al. [45] enhanced the efficiency of LHTES by using various HTF tubes configurations, including circular, square, triangular, and regular hexagonal structures. The results suggest that the triangle configuration exhibits better heat transfer efficiency in the early phase of heat transfer, mostly because to its elongated perimeter. Additionally, it can be observed that the efficiency of heat transfer is strongly correlated with the perimeter in cases when heat conduction serves as the primary source of heat transfer. Qaiser et al. [46] investigated the multi-tube LHTESU by using stearic acid as PCM. The study aims to enhance the LHTESU changing rate by changing the tube geometry and shell designs. The results show that the triangular tube configuration having vertex pointing downwards alters the melting rate of PCM 27.2% and the shell design with a 75-degree bottom vertex angle provides maximum enhancement with a 66.9% increase in melting rate.
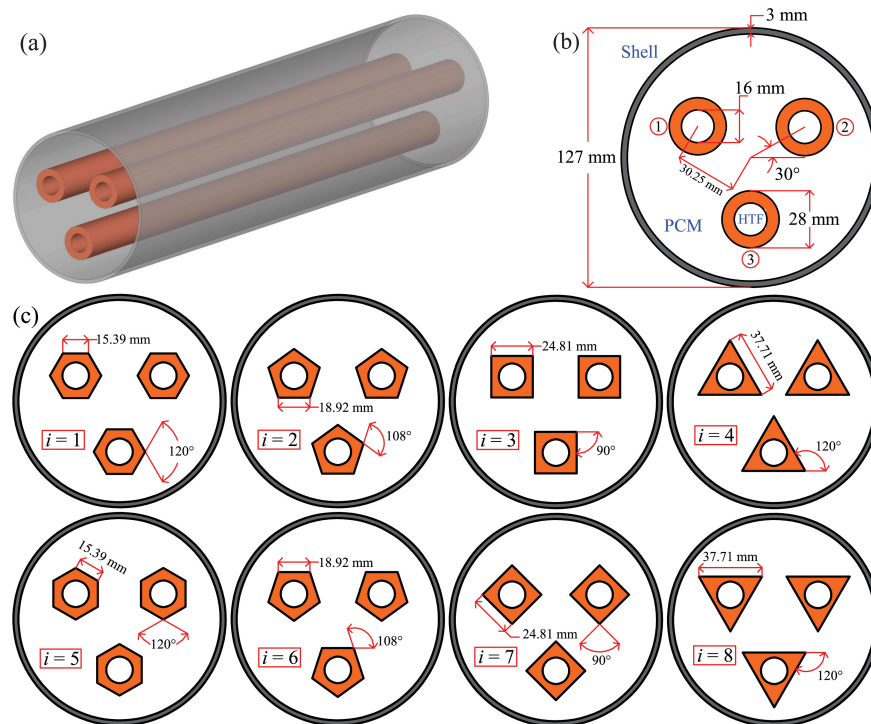
FIGURE 2.4: Schematic representation of (a) Cad model of multi-tube LHT-ESU, (b) 2D cross section of model, (c) different geometric configuration of HTF tubes. (Reprinted from Qaiser et al. [46])

Alnakeeb et al. [47] studied the effect of eccentricity of inner flat tube shell in tube LHSU for its thermal performance optimization. It was found that the eccentricity of the inner flat-tube takes part as pivotal role in dictating the efficiency of the melting process of the phase change materiel. A reduction in the overall PCM melting time was linked to an increase in the downward shift of the flat i.e. eccentricity for all flat tube configurations. Comparing the maximum eccentricity of 0.75 to the concentric circular tube case, the total charging time is reduced by 68.6%. Ghalambaz et al. [48] investigated a LHTES system that uses wave-shaped HTF tubes. This work utilizes coconut oil and nano-enhanced phase change material as the PCM. The Taguchi optimization approach was employed to determine the optimal design of the LHTESU. Research has shown that rise in the volume percentage of nanoparticles results to a decrease in the duration required for charging. Zhang et al. [49] conducted a study on a horizontal single-stream shell-and-tube TES unit as shown in Figure 2.5, where the eccentricity between the inner and outer tube was intentionally engineered to enhance the charging and discharging capabilities. A computational method utilizing a fixed grid and an enthalpy-double-porosities model is suggested for precise prediction of the melting or solidifying behavior of LTESUs with varying eccentricities. To shorten the entire melting or melting-solidifying time, certain optimum eccentricities can be achieved. The results indicate that just focusing on the charging process, vertically descending the inner tube from the center of the outer tube significantly reduces the overall charging time. Nevertheless, a higher eccentricity does not necessarily result in improved melting efficiency. Put, there is an ideal eccentricity that results in the quickest melting time. The study reveals that the ideal eccentricity for the melting process has a linear relationship with the Rayleigh number. The unconventional configuration of the inner tube is advantageous in reducing the overall time required for the melting and solidifying processes, but only if the ratio of the Rayleigh number during solidification to the Rayleigh number during melting is greater than 2.0.

Vikas et al. [50] conducted a study on the melting performance of paraffin wax in a multi-tube latent heat thermal energy storage system. A comparison is made
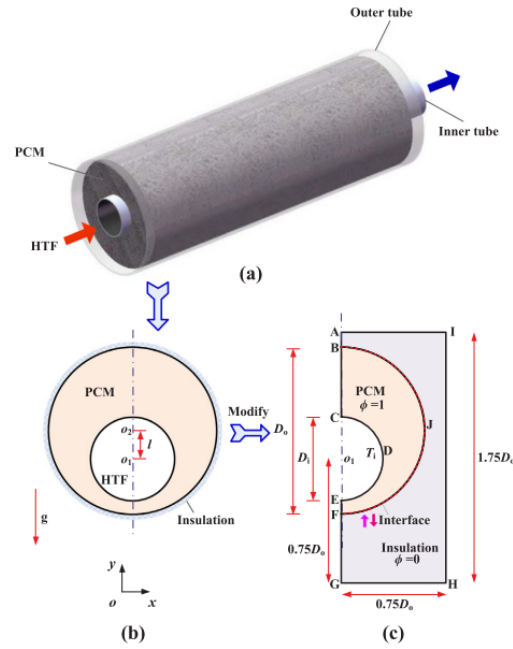
FIGURE 2.5: Schematic representation of (a) 3D Cad model of Single stream shell and tube LHTESU, (b) Cross section of Cad model, (c) Computational domain for research. (Reprinted from Zhang et al. [49])

between the performance of ten configurations of five HTF tubes. The peripheral eccentricity of 4 HTF tubes is adjusted relative to a stationary central tube. The research aims to determine an optimal configuration of several heat transfer fluid tubes while keeping constant PCM. The suggested designs are evaluated by analyzing the average liquid fraction plot, heat flux at the outer surface of the HTF tubes, and average domain velocity. The melting behaviors are significantly affected by the configuration of the tubes. Research has revealed that to slow down the process of thermal stratification, the tubes in upper half should be positioned nearer to the center, while in lower half, they should be inserted deeper into the poorly melted area. The staggered configuration of planetary tubes exhibits higher efficiency compared to the inline configuration at specified eccentricities. Case 9 and Case 1 demonstrate the most rapid and sluggish melting, with melting times of 128 and 269 minutes, respectively. The proposed designs have the capacity to store 1450 kJ/m of specific energy with a efficiency of 98%. Yusuf et al. [51] experimentally investigate the charging dynamics of paraffin in an inclined shell and tube LHTES unit. Both the concentric and eccentric alignments of the inner tube with respect to the center point of the outer shell are taken into account. The study examines three distinct eccentricity values measured from the precise center

of the outer shell: e = 10, 20, and 30 mm. The impact of the input temperature
on the process of melting behavior is determined for each geometric orientation.
Significant emphasis is placed on explaining the melting behavior by analyzing the
temporal fluctuations of the temperature field within the phase change material.
Eccentricity has been found to have a significant impact on the melting behavior
of phase change materials, leading to an enhancement in melting behavior. This
occurs due to the increased intensity of natural convection occurring within the
PCM.
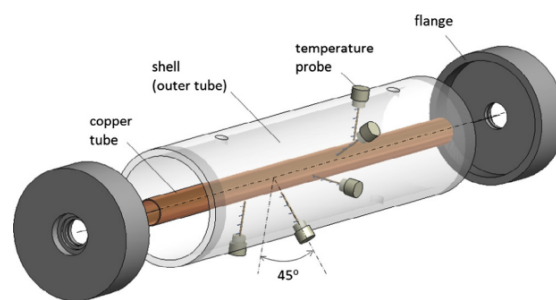
FIGURE 2.6: 3D cad model of inclined shell and tube latent heat thermal energy
storage system. (Reprinted from Yusuf et al. [51])

Esapour et al. [52] performed a numerical analysis and comparison of multi-tube
heat exchangers, examining the effects of changes in both geometric and opera-
tional characteristics. This study examines the impact of the number of tubes
and their arrangement as geometric parameters on melting fraction and melting
time. The process evolution can be observed using melting fractions and stream-
lined contours. The results indicate that conduction is the primary method of
heat transport during the initial phases of the melting process, until a stage where
convection becomes the dominant mechanism. The findings also indicate that the
configurations with tubes positioned in the upper portion of the enclosure are po-
tential candidates for experiencing the longest duration of melting. In general,
when the tubes are located in the lower region of the system, a higher rate of
melting is achieved for tubes with the same inner tube numbers. Vikas et al. [53]
conducted a numerical study to examine the charging and discharging behavior
of a latent heat thermal energy storage system comprising of a shell and several
heat transfer tubes. The purpose was to determine the most appropriate arrange-
ment of the tubes for efficient heat transfer. This research examines nine tubes

arranged in eight distinct configurations. ANSYS Fluent was used to conduct numerical simulations on a reduced two-dimensional paraffin wax domain. The transient performance is assessed by analyzing variations in melt fraction, heat transfer rate on the tube surfaces, melting time, and energy storage with time. The findings indicate that the process of charging and energy storage efficiency is significantly influenced by the arrangement of tubes. The staggered array of tubes with a high pitch-to-tube diameter ratio exhibited higher efficiency in the described cases. A 74.2% decrease in melting time is found when the tubes are arranged in a staggered array with a pitch ratio of 3.5 (S3.5 case), compared to an inline array with a PR of 2 (I2 case). The S3.5 array achieves a 9% increase in energy storage relative to the I2 array over 300 minutes of charging by rearranging the tubes. Ghalambaz et al. [48] studied the melting process of multitube LHTESU by using the RT35 as a PCM. The thermal behavior of the system was determined through the utilization of the Liquid fraction graph, streamlines, and temperature contours. The optimal location for the tubes was determined through the utilization of the Taguchi optimization methodology. The results show that the position of the tube in the enclosure plays a key role in the enhancement of LHTESU. By relocating the tubes to an optimal position within the enclosure, the rate of charging can be altered by a significant margin of 44%.

According to the authur's knowledge, there has not yet been a comprehensive study on optimizing latent heat thermal energy systems by simultaneously altering all three key parameters: the aspect ratio of the shell, the tube shape, and the position or arrangement of the tubes. This study seeks to optimize the melting time of LHTESU by considering all these constraints and proposing multiple alternatives that have the potential to improve their performance. The primary objective of this study is to enhance the performance of LHTES systems through the strategic modification of crucial design factors, including the shell geometry, tube position, and tube shape. The shell geometry involves the overall design and specifications of the storage container, which influence the rate of heat transfer and the performance of the system. The concept of tube location deals with the positioning of heat exchange tubes within the storage medium, which has a direct influence on the distribution of thermal energy. The efficiency of heat transfer inside the system

is further influenced by tube geometry, which includes factors such as diameter and arrangement. Through the study and modification of these characteristics by using Taguchi method, this study aims to achieve an optimal configuration that reduces charging time, maximizes the capacity for energy storage, minimizes heat dissipation, and enhances the overall efficiency of LHTES systems. This study also utilized Analysis of Variance to determine the percentage impact of each design aspect on the improvement of melting time and constructed a mathematical equation utilizing a linear regression model to predict the duration required for charging the LHTESU.

Chapter 3

Problem Formulation

3.1 Computational Domain Design and Thermo-Physical Properties

The computational domain consists of a 2D cross-section of a rectangular shell and tube latent heat thermal energy storage unit, as illustrated in Figure 3.1 (a). Figure 3.1 (b) shows the symmetric model of one segment of a rectangular shell and tube heat LHTESU. The copper tubes have a hydraulic diameter D_h of 29.4 mm and the thickness of HTF tubes is 2 mm. It is mounted inside a steel shell that has a height of 314.325 mm and a width of 74.243 mm for each repeated segment [48]. The clearance distance of HTF tubes at the bottom Z_{min} is 5 mm. The distance between the tubes is measured by three independent parameters as illustrated in Figure 3.1(b). These parameters define the location of HTF tubes. This study analyses the effects of three specific design variables on the melting time of the PCM. These parameters include tube geometry t_g, vertical tube placement t_l, and shell aspect ratio Ar_s The study under consideration investigates three distinct parameters as illustrated in Figure 3.2. Each arrangement exhibits a correlation with the design parameters t_g, t_l, and Ar_s. The melting rate is investigated through systematic variations in the t_g, t_l, and Ar_s.

TABLE 3.1: Thermophysical properties of Rubitherm RT-35 [54].

Property	Symbol	Value
Density (solid)	ρ_s	815 kg/m^3
Latent heat capacity	L	170 kJ/kg
Specific heat capacity	c_{ps}	2000 $J/kg.K$
Thermal conductivity	k	0.2 $W/m.K$
Dynamic viscosity	μ	0.023 $Pa.s$
Thermal expansion coefficient	β	0.0006 $1/K$
Solidus temperature	T_s	302 K
Liquidus temperature	T_l	308 K
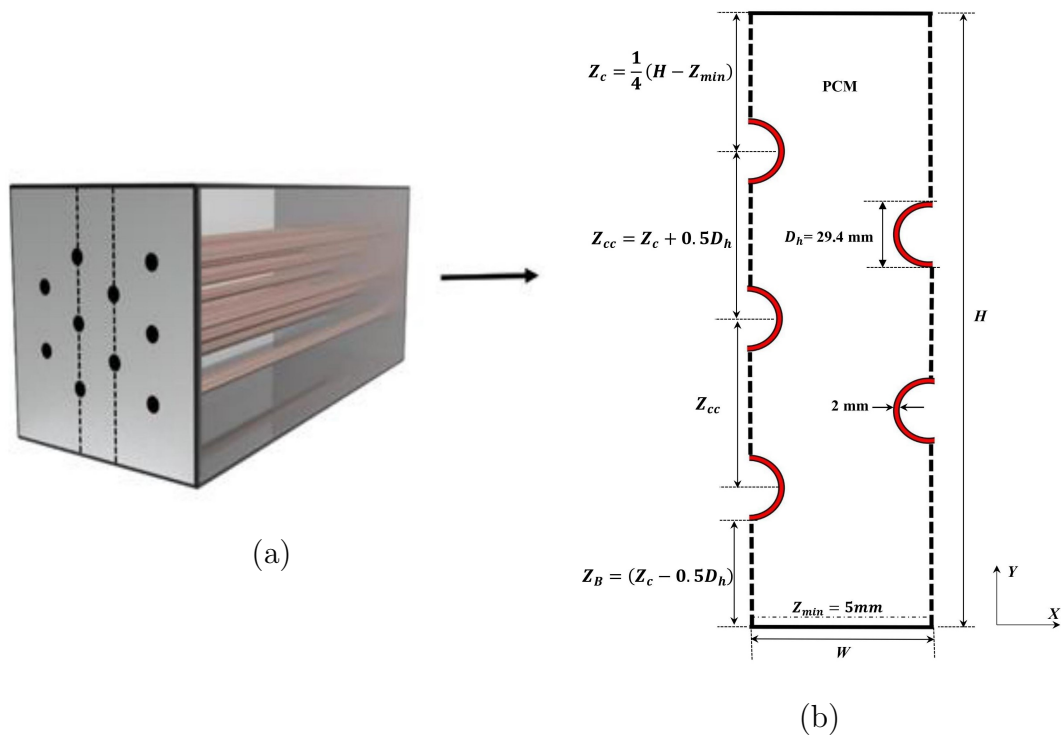
FIGURE 3.1: Schematic visualization of (a) 3D model of the base case design, (b) Symmetric model of the base case design

The overall volume of the PCM in the LHTESU remains constant for all cases considered in this study. The selected PCM for this investigation is Rubitherm RT35, chosen predominantly for its non-toxic properties, making it a suitable substitute for use as a PCM. Additionally, the temperature at which the PCM undergoes a phase change remains constant. The thermal characteristics of Rubitherm RT-35 are thoroughly detailed in Table 3.1. Nine distinct LHTESU designs are proposed, categorized depending on the design of the experiment L9 array table suggested by the Taguchi method. These nine cases incorporate various combinations of design

parameters, such as the aspect ratio of the shell, the location of HTF tubes within the shell, and the geometry of the HTF tubes. Design variations are analyzed by simulating multiple configurations of design parameters, ultimately resulting in optimized design parameters that reduce melting time. For this research, we have utilized Case 1, Case 4, Case 7, and Case 9 from the DOE L9 array table for comparison because these cases cover all the design parameters changes. Figure 3.2 illustrates the schematics of Case 1, Case 4, Case 7, and Case 9 highlighting the significant design factors.

3.2   Modelling Theories and Simplifications

The flow of liquid phase change material is considered incompressible, with Newtonian behavior, and possesses the properties of homogeneity and isotropy. The effect of radiation heat transfer is significantly smaller than the influence of natural convection phenomena. The outer surface of the enclosure is adiabatic, while the internal surface of the Heat Transfer Fluid tubes maintains an isothermal condition. The interaction region between the liquid and solid phase of a phase change material is characterized by a narrow and soft region called a mushy zone. The mushy zone is usually considered a composite state of the solid and liquid phases of PCM. When modeling the charging process of phase change materials, the Boussinesq approximation is widely used as it accurately models the impact of fluctuations in density. This approach allows numerical computations to integrate a uniform average density, ignoring phase change volumetric expansion. Vogel and Thess [55] recently analyzed the phase change phenomena using a 2D enthalpy porosity model based on constant volume. Thus, this work uses a two-dimensional constant volume enthalpy porosity model for numerical simulations with a uniform average density.
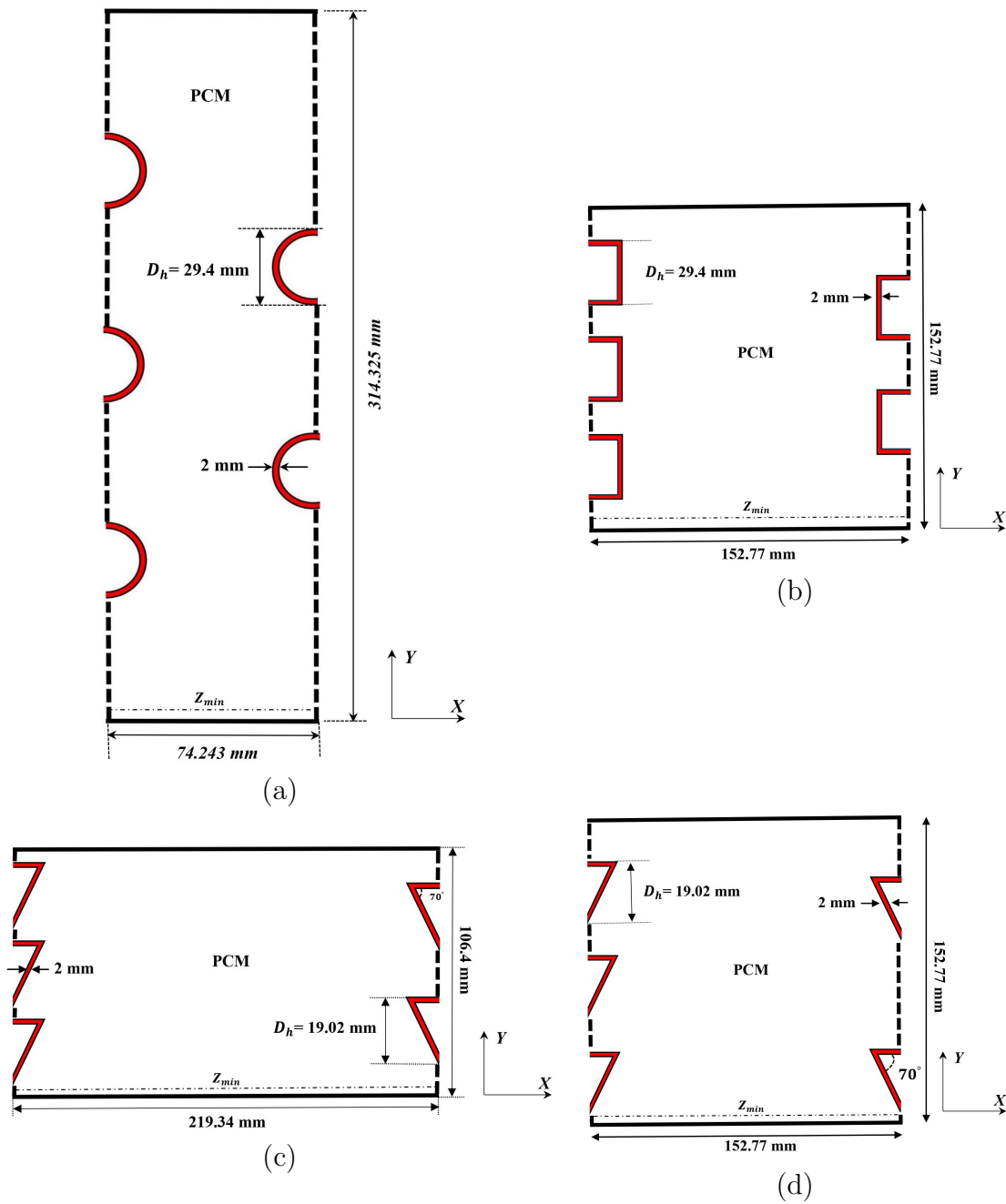
FIGURE 3.2: Schematics of symmetric models of (a) Case 1, (b) Case 4, (c) Case 7, and (d) Case 9

3.3   Governing Equations and Numerical Models

The melting process results in a buoyancy-driven flow of liquid phase change material, which is an unstable, incompressible laminar flow. The constancy of the phase changing material melting process presents a significant challenge, primarily due to the requirement of a two-phase flow which includes natural convection effects due to density differences. The induction of PCM can be achieved by the utilization of the enthalpy-porosity model developed by Voller and Prakash [56]. Equations (3.1), (3.2), and (3.3) represent the fundamental governing equations for Continuity, Momentum, and Energy, respectively.

$$\frac{\partial(\rho)}{\partial t} + \frac{\partial(\rho u_i)}{\partial x_i} = 0 \tag{3.1}$$

$$\frac{\partial(\rho u_i)}{\partial t} + \frac{\partial(\rho u_i u_j)}{\partial x_j} = -\frac{\partial p}{\partial x_i} + \mu \frac{\partial^2 u_i}{\partial x_j \partial x_j} + S_B + S_{Mi} \tag{3.2}$$

$$\frac{\partial(\rho h)}{\partial t} + \frac{\partial(\rho u_i h)}{\partial x_i} = \frac{\partial}{\partial x_i}\left(K\frac{\partial T}{\partial x_i}\right) \tag{3.3}$$

The variable u_i stands for the velocity of liquid phase change material as well as solid phase change material but for solid $u_i = 0$, where P denotes pressure, g represents gravity, μ represents dynamic viscosity, and ρ characterizes mean density. S_{Mi} stands for momentum resource. When PCM melts, the changes in density caused by the temperature and the force of gravity lead to a phenomenon called the buoyancy effect. The energy equation uses the Boussinesq approach to figure out the buoyancy source term, which is written as $S_B = \text{g}\rho\beta(\text{T-}T_l)$. In equation 3.3 the terms k, T, and h represent the thermal conductivity, temperature, and specific enthalpy. In PCMs, the change in enthalpy of phase change material includes three different phases: solid, solid-liquid coexisting, and liquid. Differentiation is represented by equation (3.4).

$$h = \begin{cases} \int_{T_i}^{T} c_{p_s} dT, & \text{if } T < T_s \\[2mm] \int_{T_i}^{T_s} c_{p_s} dT + \gamma h_\Delta, & \text{if } T_s \leq T < T_l \\[2mm] \int_{T_i}^{T_s} c_{p_s} dT + h_\Delta + \int_{T_l}^{T} c_{p_l} dT, & \text{if } T \geq T_l \end{cases} \tag{3.4}$$

T_i denotes the initial temperature at the outer surface of the tubes, which has been accurately set as 300K. Moreover, h_Δ represents the latent heat of the fusion of PCM in its solid and liquid phases, which is initially considered to be zero. The specific heat capacity of PCM in its solid state is represented as C_{Ps}, while the specific heat capacity of PCM in its liquid state is referred to as C_{Pl}. The symbol γ is utilized to represent the liquid percentage of phase change material, which functions as an indicator of the duration of the phase change phenomena. The melt fraction γ of the PCM is presented in Equation (3.5).

$$\gamma = \frac{h_\Delta}{L_{\text{PCM}}} = \begin{cases} 0, & \text{if } T < T_s \\[2ex] \dfrac{T - T_s}{T_l - T_s}, & \text{if } T_s < T < T_l \\[2ex] 1, & \text{if } T > T_l \end{cases} \tag{3.5}$$

Like the enthalpy changes, the melting fraction goes through three distinct stages:

1. When the temperature is beyond the solidus temperature of the phase change material (PCM), the fraction of the material that has melted is 0.

2. When the current temperature is higher than the temperature at which a PCM melts, the fraction of the PCM that has melted is 1.

3. When the present temperature is between the temperature at which the PCM melts and the temperature at which it solidifies, the fraction of the PCM that has melted is calculated by dividing the difference between the melting and solidifying temperatures by the difference between the current temperature and the solidifying temperature.

In equation (3.2), the momentum source term S_{Mi} denotes the varying momentum of liquid phase change material due to the natural convection effect. This source term is modeled using Darcy's law [57], which works as a momentum-dampening term. The momentum source expression is shown in equation (3.6).

$$S_{Mi} = \frac{C_{\text{Mushy}}(1 - \gamma)^2}{\gamma^3 + \epsilon} u_i \tag{3.6}$$

C_{Mushy} is the mushy zone constant that controls velocity damping. C_{Mushy} readings typically range from 10^4 to 10^7. A greater C_{Mushy} value results in a higher velocity damping rate. However, excessively high values cause large fluctuations in the solution. Based on a comparison of numerical and experimental results, the suitable value of the mushy zone constant is determined to be 10^5 [58] in this study. Because the denominator in equation (3.6) contains (γ^3), the source term can become infinite when PCM is totally solid ($\gamma = 0$). To avoid this, ϵ=0.001 is added to the denominator of S_{Mi}.

Stefan and Rayleigh numbers, crucial for characterizing the buoyancy-induced flow, are defined in equations (3.7) and (3.8) [59], respectively. Stefan number (Ste) is described as a ratio of sensible heat to latent heat of the PCM. The latent heat of the PCM is represented by L_f, the HTF tube temperature and liquidus temperature of the PCM are denoted by T_t and T_l, respectively.

$$Ste = \frac{C_{pl}(T_t - T_l)}{L_f} \tag{3.7}$$

The Rayleigh number (Ra) is a ratio of buoyant forces to viscous forces. In equation (3.8) β signifies the thermal expansion coefficient, D_h stands for the hydraulic diameter of the tube, kinematic viscosity is denoted by ν_l, and thermal diffusivity is represented by $a_{th,l}$ respectively.

$$\mathrm{Ra} = \frac{g\beta(T_t - T_l)D_h^3}{\nu_l a_{th,l}} \tag{3.8}$$

The Nusselt number is defined as a heat transfer ratio of convection to conduction. Equation (3.9) is used to get the average Nusselt number ($\overline{\mathrm{Nu}}$).

$$\overline{\mathrm{Nu}} = \frac{\overline{h_c}D_h}{K} = \frac{\dot{Q}_{stored}}{\pi K(T_t - T_{PCM})} \tag{3.9}$$

$\dot{Q}_{stored}$ is the amount of total energy storage of phase change material, which is derived by dividing the total energy stored by the total melting time of phase change material, i.e. $\dot{Q}_{stored}/m_t$. While T_{PCM} (t $= 0$) represents the PCM's initial temperature.

3.4 Discritization Schemes and Numerical Models

The mathematical equations governing PCM's melting process are solved using numerical methods, considering initial and boundary conditions for the 2D problem formulation. Numerical simulations of various LHTES unit designs are conducted by using commercial CFD software ANSYS Fluent 21.0. The solver utilizes the enthalpy-porosity model and the finite volume methods, as stated by Patankar [60]. The geometry is constructed using the Design Modeller drawing tool in Fluent. The convective term in the momentum and energy equation is solved by implementing the third-order Monotonic Upstream-centered Scheme for Conservation Laws (MUSCL), which combines the central differencing and upwind scheme. The use of this scheme results in an improvement in spatial accuracy and a reduction in numerical diffusion, leading to solution stability even when longer time steps are used. The pressure equation is solved by utilizing the PREssure STaggering Option (PRESTO!) scheme. The diffusive variable of the momentum equation is solved using a second-order central differencing scheme. Temporal discretization can be obtained by utilizing a second-order implicit scheme, which shows the property of unconditional stability. The pressure-velocity coupling in the present research is implemented using the SIMPLE technique. The under-relaxation factors for the pressure, velocity, momentum, energy, and liquid fraction are selected as 0.3, 0.2, 0.7, 1, and 0.9, respectively. The frequently accepted threshold for achieving a precise solution in terms of residual convergence is typically set at 10^{-6}.

3.5 Methods for Numerical Computation

3.5.1 Third Order Monotrocic Upstream-Centered Scheme for Conservation Laws (MUSCL)

The Third-order Monotonic Upstream-centered Scheme for Conservation Laws (MUSCL) is a computing method employed to solve hyperbolic conservation laws.

The MUSCL scheme is specifically developed to precisely capture discontinuities in the solution while simultaneously ensuring stability and computational efficiency. The MUSCL scheme is useful for modeling heat transfer and phase change processes. PCM melting is the process in which heat is transferred from a surrounding medium, such as a hot fluid or solid, to the PCM material, resulting in a phase change from solid to liquid. This process is regulated by principles of conservation, such as the conservation of energy and the conservation of mass. The MUSCL technique is capable of precisely simulating the progression of temperature and phase change boundaries within the PCM material. By enhancing the quality of the solution profile reconstruction, the technique can precisely represent abrupt temperature gradients and phase change surfaces. This is essential for accurately reproducing the melting behavior of PCM.

3.5.2 PREssure STaggering Option (PRESTO!) scheme

The PREssure STaggering Option (PRESTO!) scheme is a widely used computational method in computational fluid dynamics (CFD) simulations for solving the Navier-Stokes equations. The PRESTO! scheme is crucial for precisely simulating the fluid flow and heat transport phenomena related to the phase-change process. PCM melting occurs when heat is transferred from the surrounding medium to the PCM, causing it to change from a solid to a liquid state. The governing principles of this process are the conservation equations, which include the Navier-Stokes equations for fluid flow and the energy conservation equation for heat transfer. The PRESTO! technique employs an implicit approach to handle the connection between pressure and velocity. This method ensures computational stability and accuracy, especially in areas with significant pressure gradients, like near-phase change surfaces or fluid-solid contacts during PCM melting.

3.5.3 Enthalpy-Porosity Model

Phase change materials melting involves the use of the idea of enthalpy, which represents the internal energy of a system, in combination with the porosity of a

material experiencing phase change. Porosity is the measure of the proportion of the solid and liquid portions within a PCM material.

The enthalpy-porosity model considers the PCM as a medium consisting of many phases, including both solid and liquid phases, which exist simultaneously during the process of melting also EPM monitors the enthalpy of the phase change materials, encompassing both the sensible heat (related to changes in temperature) and latent heat (related to changes in phase). The enthalpy of the phase change material is determined by its temperature and state. The EPM incorporates the idea of porosity to quantify the proportion of the solid and liquid components within the PCM. Porosity is a crucial factor that affects how heat and mass are distributed within a material during phase shift.

3.5.4 Semi-Implicit Method for Pressure Linked Equation (SIMPLE)

The SIMPLE approach employs a method of separating the pressure and velocity computations to resolve the pressure-velocity coupling issue. The technique is continuous and consists of two steps. First, the velocity field is predicted using the previous pressure field. Then, the pressure field is updated depending on the velocity prediction. In the SIMPLE approach, the pressure corrections are handled implicitly, ensuring that the pressure correction equation is completed in a way that considers the interdependence between the pressure and velocity fields.

The implicit treatment of this issue ensures the preservation of numerical stability. The SIMPLE approach enables the use of diverse boundary constraints and source variables, which are crucial for effectively simulating PCM melting. The boundary conditions encompass heat flux conditions at interfaces between solids and liquids, interfaces involving phase transition, and convective heat transfer at interfaces between fluids and solids. Source terms refer to the energy that appears or is absorbed during a phase shift, which is often known as latent heat.

3.6   Initial Boundary Conditions

Figure 3.3 provides an outline of the parameters that must be specified for the initial boundary conditions to carry out simulations. The uniform temperature is applied at the inner surface of the heat transfer fluid (HTF) tubes and subjected to an isothermal wall boundary condition, which has a uniform temperature of 368 K. A coupled boundary condition is enforced at the contact where the outer surface of the HTF tubes meets the PCM. The above condition is valid at the starting time (t) equal to zero, whereby the external temperature is represented as T_{os} and is equivalent to the temperature of the PCM (T_{PCM}). This property applies to later cases where time (t) is greater than zero, as referenced in [61].

$$-k_{os}(x\frac{\partial T_{os}}{\partial x} + y\frac{\partial T_{os}}{\partial y}) = -k_{PCM}(x\frac{\partial T_{PCM}}{\partial x} + y\frac{\partial T_{PCM}}{\partial y}) \qquad (3.10)$$

The outer surface of the heat transfer fluid tubes has an initial temperature of 300 K, which is equivalent to the initial temperature of the solid PCM. Shell conduction is a thermal conduction phenomenon that enables the transfer of heat within a wall. This phenomenon develops when the thickness of the wall is relatively not adequate in comparison to the overall geometry. The outer walls of the enclosure are set to be adiabatic walls to minimize thermal dissipation from the molten PCM. This is achieved through the implementation of insulation on the external surface of the enclosure. Additionally, the no-slip boundary condition is imposed on both the exterior surface of the HTF tubes and the internal surface of the enclosure

3.7   Mesh and Time-Step Independence

To prevent any spurious impacts on the results due to mesh element and time-step size resolution, an independence analysis between mesh element and time-step size is conducted. Three simulations have been performed to evaluate the impact of mesh element size on the liquid fraction results as shown in Figure 3.5 (a). In this study, three different mesh sizes were chosen and the calculations were
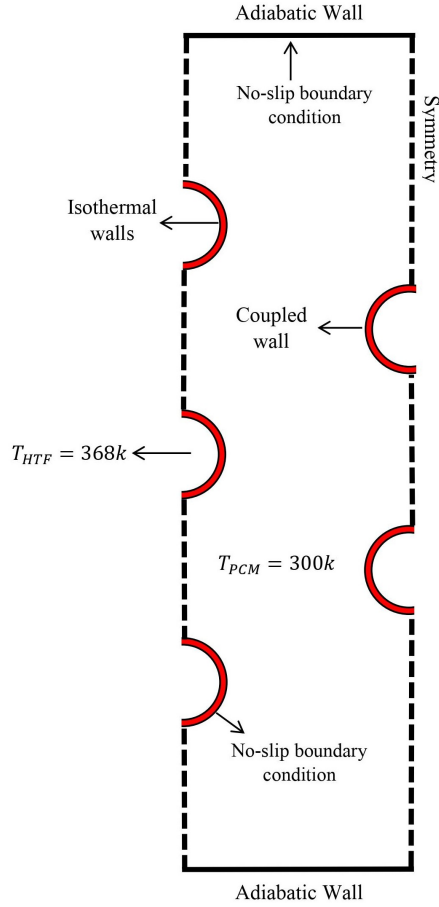
FIGURE 3.3: Boundary conditions of symmetric LHTESU model

subsequently performed for each mesh size for 16.66 mins.

The base case (Case 1) from the L9 table was used for the mesh independence analysis in the mesh study. The calculations were performed using a time step size of 30 ms. The details of mesh sizes and the quantity of grid points were as follows: coarse had 40,000, moderate had 50,000, and dense had 60,000. Multi zone quadrilateral triangular method is selected for meshing as shown in Figure 3.2. It is evident from Figure 3.4 (a) that the results of moderate and dense mesh exhibit a similarity, with less than 5% error as shown by error bars. Therefore, moderate mesh was chosen for the computational analysis.

The study investigated the effect of the time-step size on the liquid fraction melting rate as illustrated in Figure 3.5 (b) using moderate mesh for 16.66 mins. Three time-step sizes of 10 ms, 20 ms, and 30 ms were analyzed. Decreasing the time-step size leads to a significant rise in computational cost due to the significance of solving and obtaining convergence of the governing equations at each time interval. The results show that the impact of the time step variation on the computed
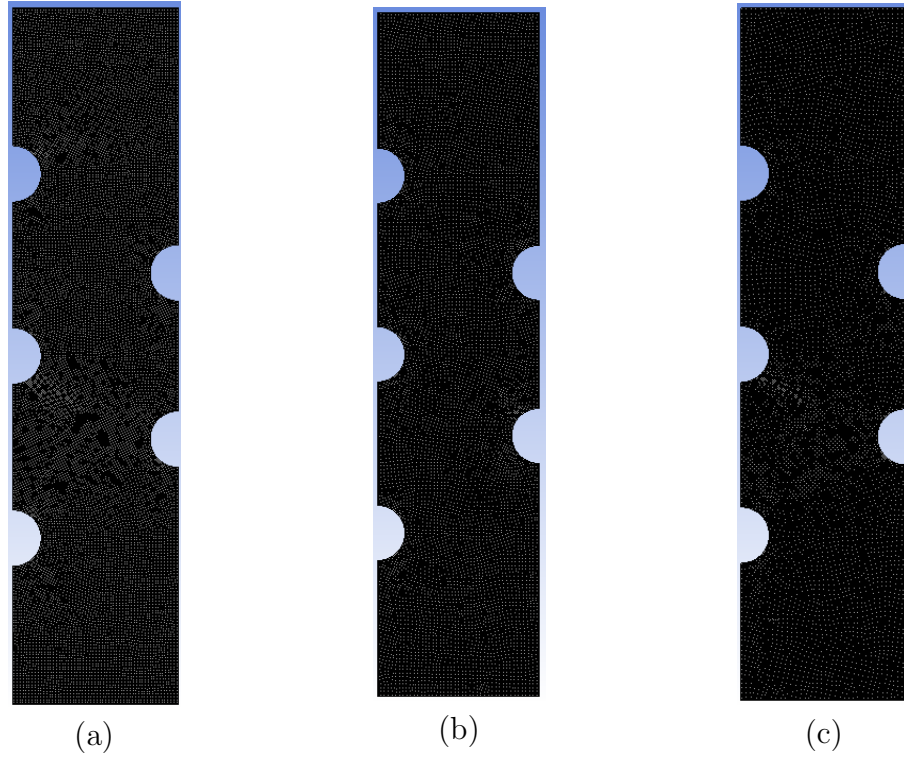
FIGURE 3.4: Mesh details (a) Coarse, (b) Moderate, (c) Dense
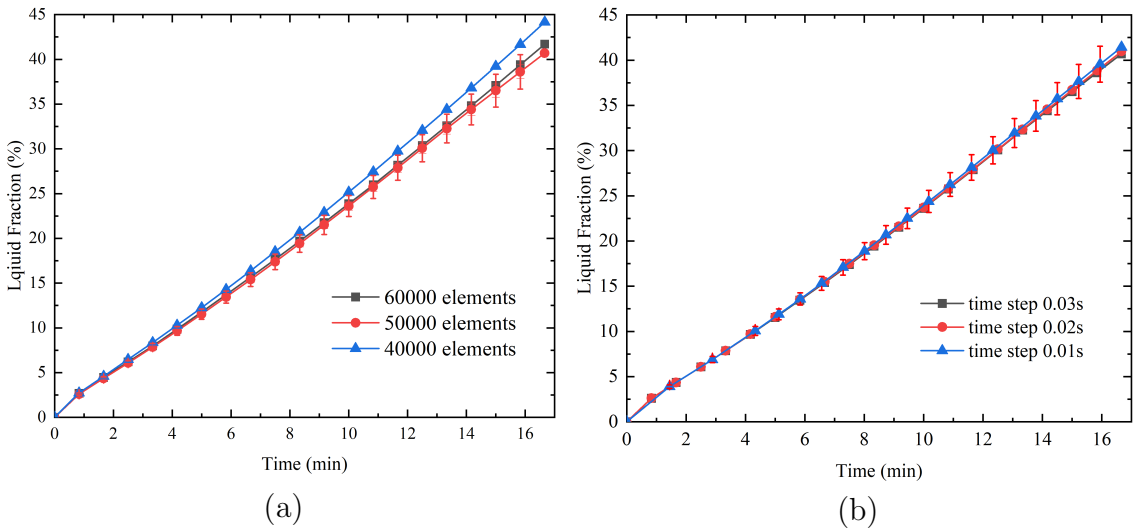
FIGURE 3.5: Mesh and time-step size independence (a) Mesh Size (b) Time-step size

melting fraction is very small and the error percentage between all three time step sizes is less than 5%. Therefore, a time step of 30 ms was chosen for all simulations conducted in the present research. It is important to mention that, after the study of time-step size, it is determined that using a time-step size of 30 ms for the mesh independence study is acceptable.

3.8 Analysis of Numerical Methods for Validity

The present numerical method's validation approach involves comparing the obtained results with previous research and regenerating the studied geometry using the same geometric and operational parameters. The multi-tube rectangular-shaped shell and tube heat exchanger are utilized. The height of the heat exchanger was 314.3 mm, the width of each symmetric segment was 74.2 mm, the thickness of the HTF tubes was 3.175 mm and the diameter of the HTF tubes was 25.4 mm. Rubitherm (RT35) is used as the phase change material. The HTF tubes that run through the shell are considered to be isothermal. Initially, the PCM is kept at a temperature of 288K, while the HTF tubes are at a constant temperature of 323K. The outer walls of the rectangular shell are set to be adiabatic and constant wall temperature is used as the boundary condition. This is similar to the boundary conditions used in our study for melting the PCM. For the validation of the current methodology, the temporal variation of the liquid fraction of phase change material is compared to that observed in [62] as shown in Figure 3.6. It can be observed that the liquid fraction graph of the present methodology precisely flows the trend of the liquid fraction graph of literature with less than 5% error in results.
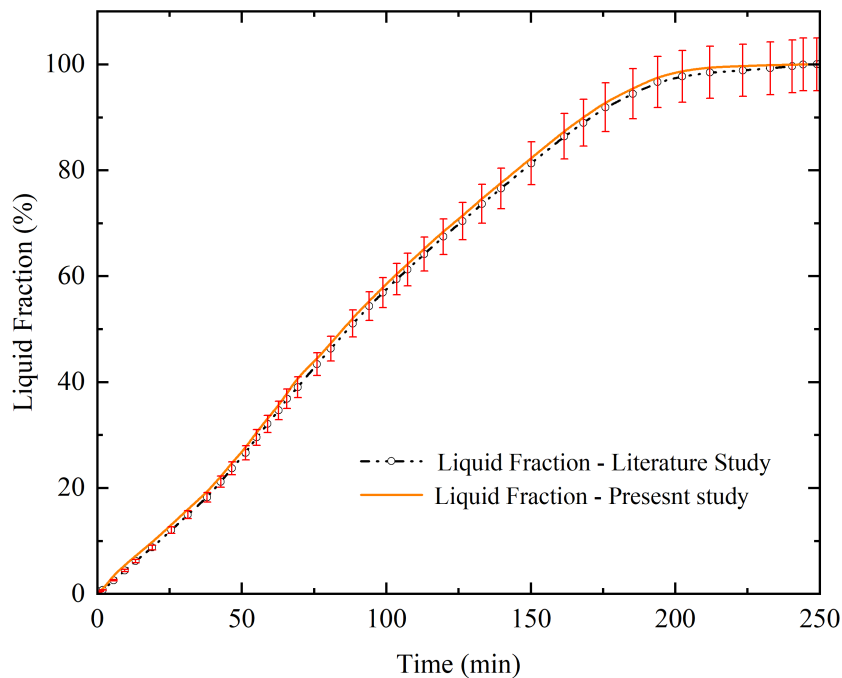
FIGURE 3.6: Comparison melting fraction plot of the present study and the numerical data of Ghalambaz et al [62] with 5% error bars.

Chapter 4

Design Optimization of LHTESU for Minimum Melting Time by Using Taguchi Method

The Taguchi Method provides a systematic approach for identifying and optimizing the design factors that have a major impact on the charging time. Latent heat thermal energy storage units (LHTESUs) are essential components in thermal energy systems. They effectively store and release thermal energy for various uses, including space heating, solar energy storage, and industrial processes. Minimising the duration required to charge a LHTESU is essential for improving the overall effectiveness and functionality of thermal energy systems. Reduced charging time enables quicker storage and retrieval of energy, which is crucial in situations that need rapid response and abundant energy supply. The Taguchi Method offers a structured approach to optimise the design parameters of an LHTESU in order to minimise the charging time. This optimisation takes into account several elements like material qualities, geometry, operating circumstances, and thermal characteristics. Engineers can quickly explore the design space, discover significant components, and find the best amounts of these elements to accomplish the intended performance objectives by running a series of structured experiments using Taguchi's orthogonal arrays.

4.1 Taguchi Analysis

The key objective of this study is to enhance the efficiency of the LHTESU by optimizing the 75% melting time. This optimization is achieved through the utilization of the Taguchi technique. The Taguchi method is a popular way to optimize because it requires a few experiments to find the best options for the factors that affect the output results. An Analysis of Variance is utilized to find out the percentage contribution of each design parameter in the enhancement of melting time. Figure 4.1 is a flowchart that shows the steps that have been taken during the optimization process. The phenomenon of free convection flow is primarily observed in the liquid PCM during the melting process, due to the effects of buoyancy forces and free convection making melting faster. Since liquid PCM frequently rises and the top of an enclosure is always exposed to large eddies, free convection heat transfer often leads to uneven melting in an LHTES unit. Because of this, energy storage systems need to be well made so that they can allow maximum use of natural convective heat transfer.
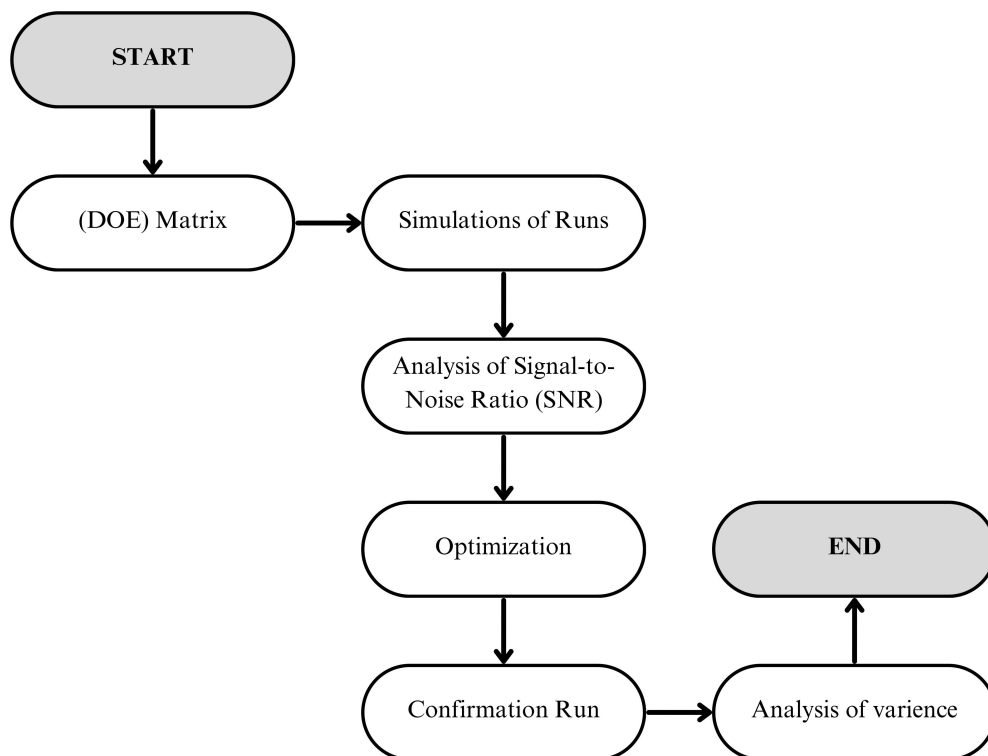
FIGURE 4.1: Flowchart of Taguchi optimization method

In the current study, the location of the HTF tubes t_l, tube geometry t_g, and the aspect ratio of the shell A_{rs} are used as design parameters. Table 4.1 demonstrates the categorizing of each design parameter into multiple levels that are useful and appropriate. Levels 1, 2, and 3 are the three separate design factors that include different design parameter configurations. Detailed information about the three different levels of each design parameter is described in Table 4.2.

TABLE 4.1: The sub-levels of design parameters

Parameters	Level 1	Level 2	Level 3
Tube geometry (t_g)	Circular	Square	Triangular
Tube location (t_l)	Z_B	$0.5Z_B$	Z_{min}
AR of shell (A_{rs})	4.23	1	0.48

TABLE 4.2: Details of controlled design parameters

Parameters	Level 1	Level 2	Level 3
Tube geometry (t_g)	1	2	3
Tube location (t_l)	1	2	3
AR of shell (A_{rs})	1	2	3

The Table 4.2 design framework is utilized to build an orthogonal table that facilitates the optimization process of the design parameters. In this study, a 3-parameter, 3-level design is selected, which consists of two arrays of distinct patterns L9 and L27. The Taguchi technique aims to optimize the design process by minimizing the number of required numerical simulations. In the Taguchi method optimization, we adopted the L9 array design to reduce the computational cost. The computation process of PCM melting, along with convective heat transfer, has been time consuming. Due to the significant time investment required for this simulation, any reduction in its duration would be of considerable assistance. Table 4.3 presents an overview of the results obtained from the L9 trial. Table

4.3 displays various LHTES configurations, where in alterations have been made to the tube geometry, HTF tube location, and enclosure aspect ratio. Each line in the table represents a distinct configuration. Ultimately, the optimization objective of achieving 75% of the charging process was selected. Therefore, it would be valuable to implement a design that can achieve a 75% PCM melting rate in half the current duration. In the Taguchi method, we have selected the principle of "the smaller, the better" approach for the signal-to-noise ratio.

TABLE 4.3: Taguchi L9 orthogonal table for three geometrical design variables and three levels.

Case No.	t_g	t_l	A_{rs}	m_t (s)	S/N Ratio
1	1	1	1	4851.6	-73.7106
2	1	2	2	2842.6	-69.0743
3	1	3	3	2825.4	-69.0216
4	2	1	2	3178.8	-70.0452
5	2	2	3	3037.2	-69.6495
6	2	3	1	2660.4	-68.4989
7	3	1	3	2980.2	-69.4849
8	3	2	1	2167.3	-66.6943
9	3	3	2	1956.6	-65.8303

After simulating all of the cases of the L9 array, the 75% melting time m_t was obtained as shown in Table 4.3. Subsequently, the Taguchi optimization method was employed to determine the significance of each case based on the signal-to-noise (S/N) ratio. The logarithmic transformation with a smaller-is-better approach was adopted, and the mathematical model for the S/N ratio is represented by equation 4.1.

$$S/N = -10 \log(\frac{\sum m_t^2}{n}) \tag{4.1}$$

The variable m_t denotes the average duration of 75% melting for all the cases, while the parameter n represents the maximum possible number of observations, which

in the present study, is limited to one. A small signal-to-noise ratio can potentially enhance the efficiency of the charging process because it minimizes the response and has data characteristics of non-negative with a target value of zero. S/N ratios are utilized in the creation of Taguchi relationships and the corresponding ranking Table 4.4. A larger difference between the highest and lowest average response values for each design factor (Delta) indicates a significant improvement in rankings. Table 4.3 demonstrates how altering each design variable affects the melting rate of the PCM in LHTES systems. Based on the analysis of Table 4.4, the primary focus of the design is the aspect ratio of the enclosure. Consequently, the location and geometry of HTF tubes became essential elements of the design process. The data presented in Table 4.4 are used to employ the Taguchi technique to figure out the optimum configuration levels for the design parameters. The results from the table are used to predict the optimum configuration levels as illustrated in Figure 4.2.

TABLE 4.4: The rank values of the control parameters based on the S/N ratio.

Level	Shape	Position	A.R
1	-69.05	-68.61	-69.18
2	-68.68	-69.56	-67.53
3	-68.16	-67.72	-69.18
Delta	0.89	1.65	1.85
Rank	3	2	1

Table 4.5 shows the Taguchi predicted design parameter levels based on the results from the means of S/N ratios plot shown in Figure 4.2 and the 75% melting time of the optimum configuration of the LHTES system.

TABLE 4.5: Taguchi method predicted optimum levels and melting time.

t_g	t_l	A_{rs}	Melting time	S/N Ratio
3	3	2	2033.64	-66.1654
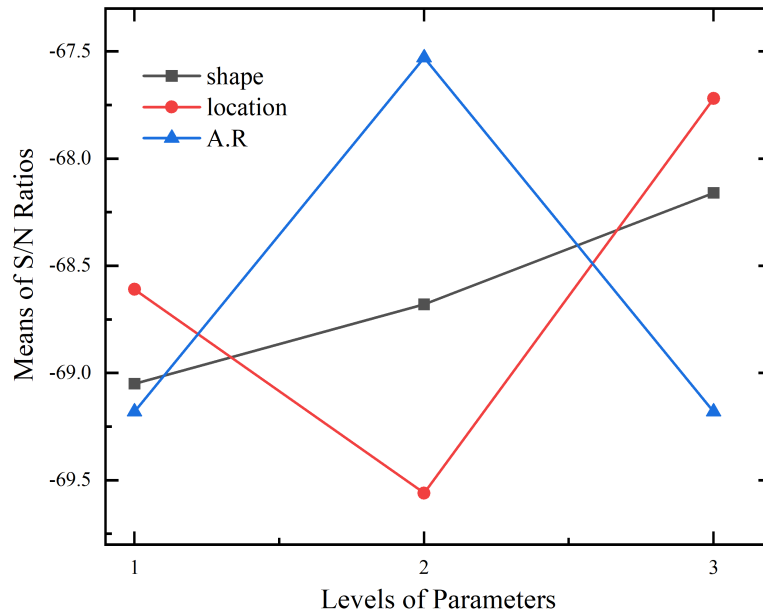
FIGURE 4.2: S/N ratio means plot for optimum levels prediction for LHTES unit design.

4.1.1 Comparison of Taguchi Prediction and Simulation Results

The optimum configuration predicted by Taguchi is replicated in Case 9 of the L9 array table. Figure 4.3 shows the three-dimensional (3D) model and two-dimensional (2D) symmetric model of the optimal Case 9. In most cases, the best solution is either one of the designs in the L9 array table or one of the designs in the table, which contains all 27 cases. In this scenario, the expected S/N ratio was utilized to estimate and validate the response at predicted optimum design parameter configurations and equation 4.2 was employed to arrive at those numbers.

$$\epsilon_{predicted} = \epsilon_l + \sum_{i=1}^{x}(\epsilon_0 - \epsilon_l) \tag{4.2}$$

Here ϵ_l represents the total mean of signal-to-noise ratio, ϵ_0 represents the mean signal-to-noise ratio at an optimal level and x describes the number of input process parameters. Table 4.6 shows the comparison between the results of Case 9 from the L9 array performed during numerical analysis and the optimum configuration predicted by the Taguchi optimization technique. Results show that the percentage

error for melting time and signal-to-noise ratio is less than 5% so Case 9 from the L9 array is selected as the optimum configuration.
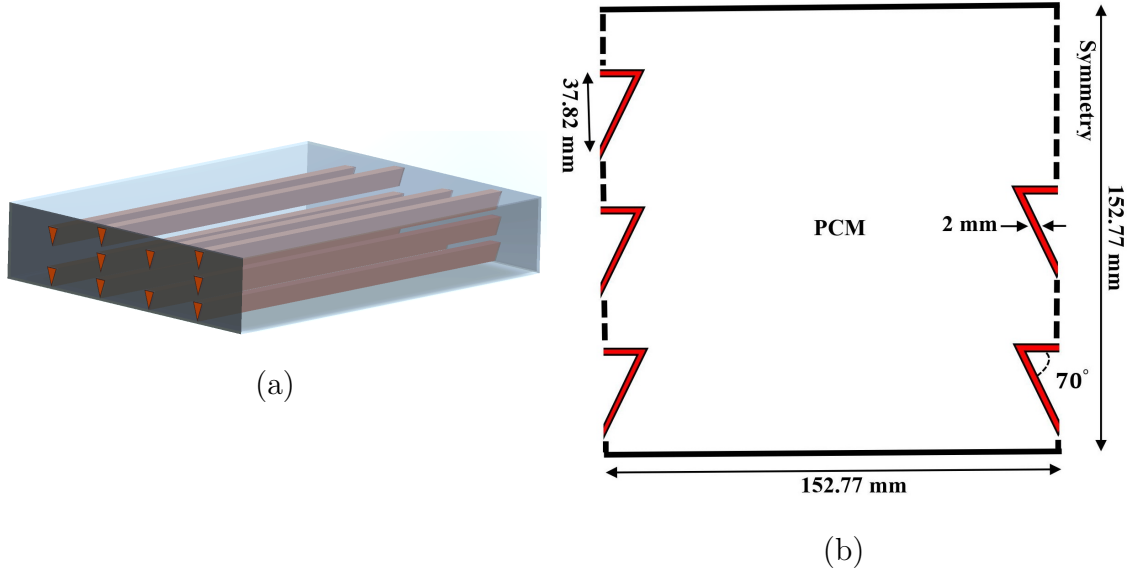
FIGURE 4.3: Schematic visualization of (a) 3D model of optimum Case 9, (b) 2D symmetric model of optimum Case 9.

TABLE 4.6: Comparison of results of Taguchi predicted configuration and Case 9 of L9 array

	t_g	t_l	A_{rs}	m_t (s)	S/N Ratio
Taguchi prediction	3	3	2	2033.64	-66.1654
Case 9	3	3	2	1956.66	-66.8303
Error (%)				3.78%	0.5%

4.2 Contribution of Design Parameters in Optimum Performance of LHTES

An Analysis of Variance (ANOVA) is conducted to evaluate the relative impact of design parameters on melting time m_t and to determine the percentage contribution of each design parameter in the enhancement of LHTESU. The signal-to-noise ratio data obtained by the Taguchi optimization technique is utilized in the

ANOVA process. To confirm the validity and dependability of the methodology, this study uses an analytical technique to create an evaluation confidence level of 95%. This means that the probability value (P) for each source must be less than 0.05 to demonstrate its significance in enhancement. Table 4.7 displays the ANOVA outcomes for melting time.

In Table 4.7 Df represents the degree of freedom, Seq ss represents sequential sums of squares, Adj ss describes adjusted sums of squares and Adj ms describes the adjusted mean squares. It is clear from Table 4.4 that the melting time varies depending on the aspect ratio of the shell (A_{rs}), location of HTF tubes (t_l), and geometry of HTF tubes (t_g) because the P value of these factors is less than 0.05. Table 4.8 shows that the percentage contribution of the aspect ratio, tube location, and tube geometry in the enhancement of the melting time of LHTESU were 41.88 %, 39.43 %, and 18.69 %, respectively. The outcomes of the ANOVA analysis revealed that the melting time was significantly affected by the enclosure aspect ratio.

TABLE 4.7: Analysis of variance for melting time signal-to-noise ratio

Source	Df	Seq ss	Adj ss	Adj ms	F	P
Shape of tube	2	2.362	1.193	0.5967	1.97	0.019
Position of tube	2	5.115	5.115	2.5576	3.15	0.037
A.R of shell	2	5.433	5.433	2.7167	4.41	0.043
Residual	2	1.231	1.231	0.6156		
Total	8	10.973				

TABLE 4.8: Percentage contribution of design variables for melting time enhancement

Variables	Contribution (%)
A_{rs}	41.88 %
t_l	39.43 %
t_g	18.69 %
Total	100 %

4.3 Linear Regression Analysis for Predictive Mathematical Model

A predictive mathematical model for the dependent variable melting time m_t as a function of the geometry of the HTF tubes (t_g), the location of the HTF tubes (t_l), and the aspect ratio of the shell (A_{rs}) was developed using linear regression analysis in the Minitab 21.0 application. The equation indicating the regression analysis is shown in equation 4.3 for melting time (m_t).

$$m_t = 3069(t_g) - 116(t_l) - A_{rs} \tag{4.3}$$

Here t_g value is the diameter of the HTF tube or hydraulic diameter of the HTF tube, t_l value is the distance between tubes and A_{rs} value is the aspect ratio of the shell. The R^2 coefficient was used to test the reliability of the evolving model. The value of the coefficient of dedication might be anything from 0 to 1 but when it's very close to 1, it indicates that the dependent and independent variables are very well-fitted. Present studies have shown that the R^2 of the refined regression model for melting time is 93.83 %. The residues were used to verify the predictive design's coefficient significance. If the range of the recurrent plot is straight, then the rest of the model errors have a normal distribution, and the design coefficients must be meaningful.

The residual graph for melting time is shown in Figure 4.4. The residuals in Figure 4.4 are close to the straight melting time range and show a central tendency at zero, indicating that, on average our projections are free from bias. There is no continuous overestimation or underestimation of the melting time, indicating the significance of the created model coefficient design. The error bars represent the level of precision or confidence associated with the expected melting timings. A 5% error bar indicates that there is a 95 percent confidence interval surrounding the predicted melting time.
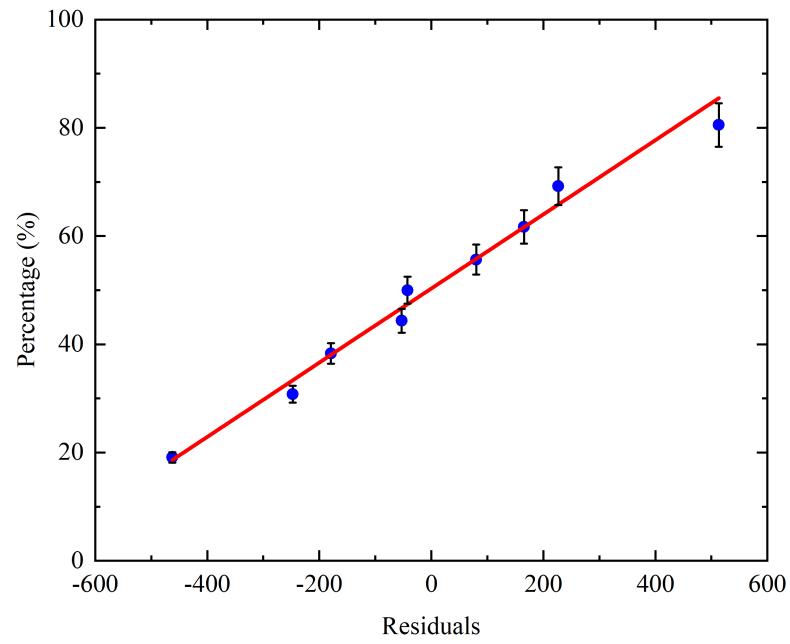
FIGURE 4.4: Normal Probability Plot of the residuals for melting time with error bars plotted at 5 percent.

Chapter 5

Results and Discussion

The simulation cases are established for the base case 1 and other eight cases suggested by the Taguchi L9 array table. The geometric characteristics and initial boundary conditions are precisely defined as described in previous sections. Simulation studies are conducted under various design settings to analyze the effects on temperature transfer and melting enhancement for all nine cases but for comparison purposes, Case 1, Case 4, Case 7, and Case 9 are selected from the L9 array table. The results section explores many performance enhancement metrics and determines the optimal design. also, this section discusses the capacity and rates of energy storage for four designs out of total nine cases. Furthermore the effects of different HTF temperatures on melting time of optimum Case 9 is presented by using non-dimensional Stefan, Rayleigh and Nusselt numbers.

5.1 Transient Melting Process of LHTESU

The melting rate and temperature distribution in the LHTES system during the charging Process of Case 1, Case 4, Case 7, and Case 9 are illustrated in Figure 5.1. These LHTES configurations incorporate all critical design parameter variations that affect the melting process. Figures 5.1 (a, b) show the average melting fraction and average temperature distribution plots of Case 1, Case 4, Case 7, and Case 9. The melting and temperature plot of Case 9 shows that Case 9 reaches

higher melting rates and temperatures as compared to Case 1, Case 4, and Case 7. Initially, when (t < 2 mins) the melting rate of PCM is observed to be linear and identical for all the cases due to the conduction dominant heat transfer and the LHTES system temperature is below the PCM melting temperature. Initially when the melting process starts natural convection flow appears inside the enclosure and the melting region stretches far away from the HTF tubes. Therefore, the aspect ratio of the shell (A_{rs}) and HTF tube location (t_l) can somehow manage the convection movement and control the temperature distribution and convection flow in a streamlined flow. Heat transfer within the enclosure occurs through the conduction mechanism because, at the initial stage, convection effects are ineffective. After t > 5 min, variation starts to occur in melting and temperature graphs because buoyancy effects kick in, and natural convection effects become prominent and PCM at the top of the enclosure melts. The latent heat of liquid PCM is absorbed by solid PCM and continues to create a larger melted zone as shown in Figure 5.2 (a). The phase change material around the HTF tubes exhibits characteristics of a large domain. In all design Cases except the optimal Case 9, the thermal conductivity of PCM is reduced because the gap between the HTF tubes is large enough and there is no mutual influence between them. Therefore, when t > 20 mins evident variation occurs in melting and temperature plots because at that time mostly the upper portion of the enclosure is melted as shown in Figure 5.2 (a), and convection current in the phase change material and surrounding medium is affected by the distribution of heat. The conduction mechanism inside the molten PCM and solid PCM also leads to the variation in the graph.

Figure 5.1 (b) illustrates the average temperature plot of Case 1, Case 4, Case 7, and the optimum Case 9. The average temperature fluctuation is less significant compared to as observed in the liquid fraction. The average temperature of phase change material remains constant for approximately the first 3 minutes. There is a noticeable variation in temperature after 5 minutes. Liquid PCM moves towards the bottom because liquid PCM has low density and viscosity and solid PCM absorbs latent heat stored in liquid PCM through conduction and starts to melt and create recirculation zones. The thick melting layer is formed between Solid and liquid PCM because of the enhanced natural convection and close contact melting

phenomenon. Figure 5.1 illustrates the 75% phase change material melts at 32.61 mins and the PCM average temperature is 331.53 K for optimum Case 9 while at that time base Case 1 reached 56% melting and the PCM average temperature is 318.26K which shows the optimum Case 9 is more efficient. Similarly, Case 4 reaches 62% melting and PCM average temperature is 322.4K, and Case 7 reaches 71% melting and average PCM temperature is 327.61K. Thus, as illustrated in Figure 5.1 (c), Case 9 has the shortest melting time m_t, while Case 1 has the longest, and Case 4 and Case 7 have trends of melting between Case 1 and Case 9. Figure 5.1(d) shows that the nusselt number increases with the variation of geometry from case 1 to 9. As we optimize the geometry it can be seen that for the case 9, the nusselt number is highest having the strongest convective heat transfer as compared to conduction.
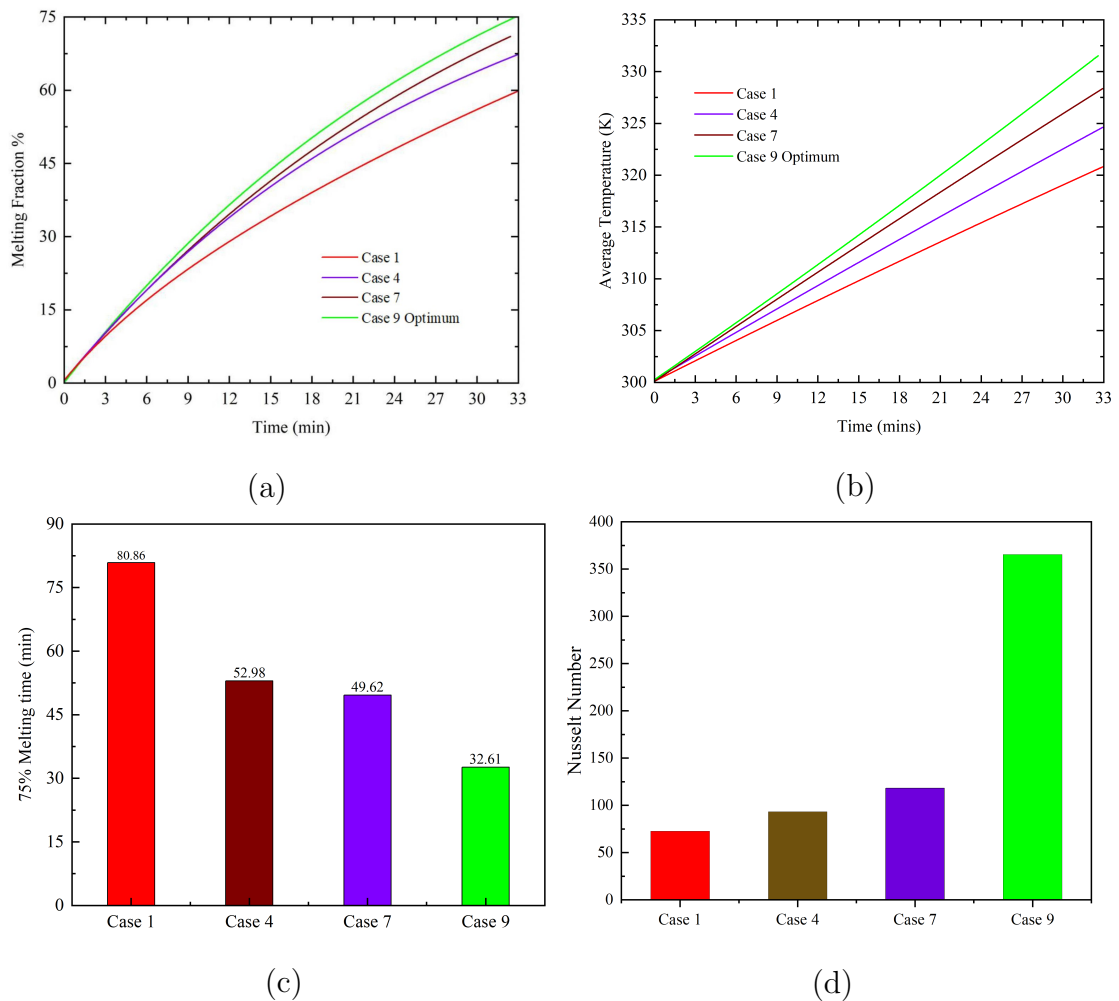

FIGURE 5.1: Comparison of different design configurations of LHTESU (a) average melting fraction of PCM, (b) average temperature of PCM, (c) melting time of PCM, (d) Nusselt number.

The study of the melting process and temperature distribution involves analyzing the contours of the liquid fraction and temperature distribution. Figure 5.2 and 5.3 demonstrates the contours of 75% melting and temperature distribution of Case 1, Case 4, Case 7, and Case 9 from the L9 table design. Figure 5.1 shows that optimum configuration Case 9 reaches 75% melting in just 32.61 minutes while at that time Case 1 is at 56%, Case 4 is at 62% and Case 7 is at 71%. The contours are plotted at different time steps during the charging process as illustrated in Figure 5.2 and 5.3. The influence of natural convection is evident in the melting fraction and temperature distribution contours from the start. The convection phenomena increase the temperature of the phase change material in the upper region, resulting in improving the melting rate of the PCM in that region. The dark blue region in the melting contour in Figure 5.2 represents the solid PCM, while the dark red region indicates the liquid PCM. The thick line separating these two regions represents the melting interference line. Figures 5.2 illustrate that rapid melting takes place in nearby areas of the HTF tubes, causing the liquid PCM to flow toward the gap between the tubes. Once all of the area surrounding the tubes is filled with liquid PCM, it proceeds to rise toward the uppermost portion of the enclosure due to the influence of buoyancy forces. During the flow of HTF through the tubes, it is evident that a melting region forms around all of the tubes. The melting zone is enhanced as the tubes get closer to one another. As illustrated in Figure 5.2, solid PCM undergoes a phase change to a liquid state in the area of the tubes due to the increased temperature.

When t>13.33 mins it can be seen that the local regions around the hot tubes are completely molten and merged but the upper and lower portions of the enclosure are still in a slightly solid state. The reason for this is that the bottom zone in Case 1, Case 4, and Case 7 is just under the influence of a single tube and the location of other tubes cannot create a significant effect on the bottom of the LHTES. In optimum Case 9, the bottom zone is under the influence of multiple tubes and shows a significant impact on the melting of PCM which shows that the movement of tube location towards the bottom of the enclosure creates a significant impact and also creates the melting interface upwind. The results show that in Case 1, Case 4, and Case 7 central region of the enclosure is at high temperature except in the optimum Case 9. In optimum Case 9, illustrated in Figure 5.2, the upper

area is observed to have a high temperature, which directly affects the melting rate of PCM. Additionally, the heat released by the HTF tubes is utilized as latent heat. In optimum Case 9 the uppermost portion experiences melting while a minor quantity of the PCM in its solid state remains situated at the lowermost part.

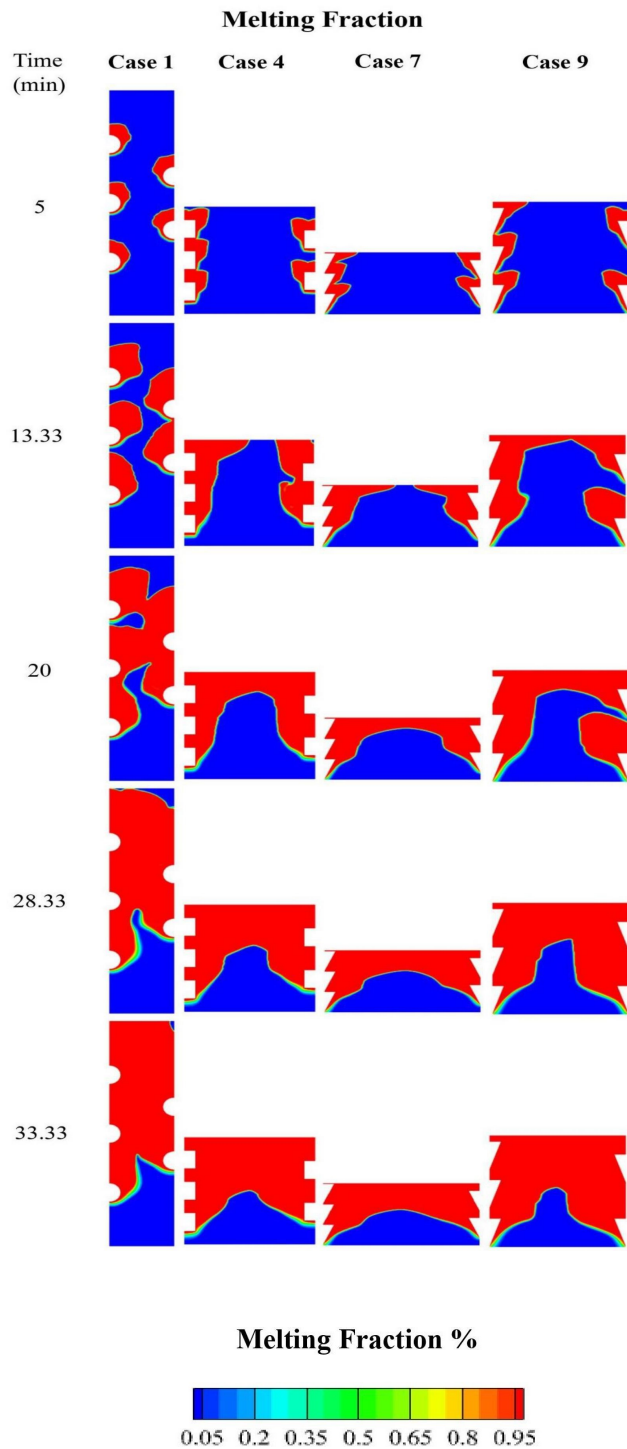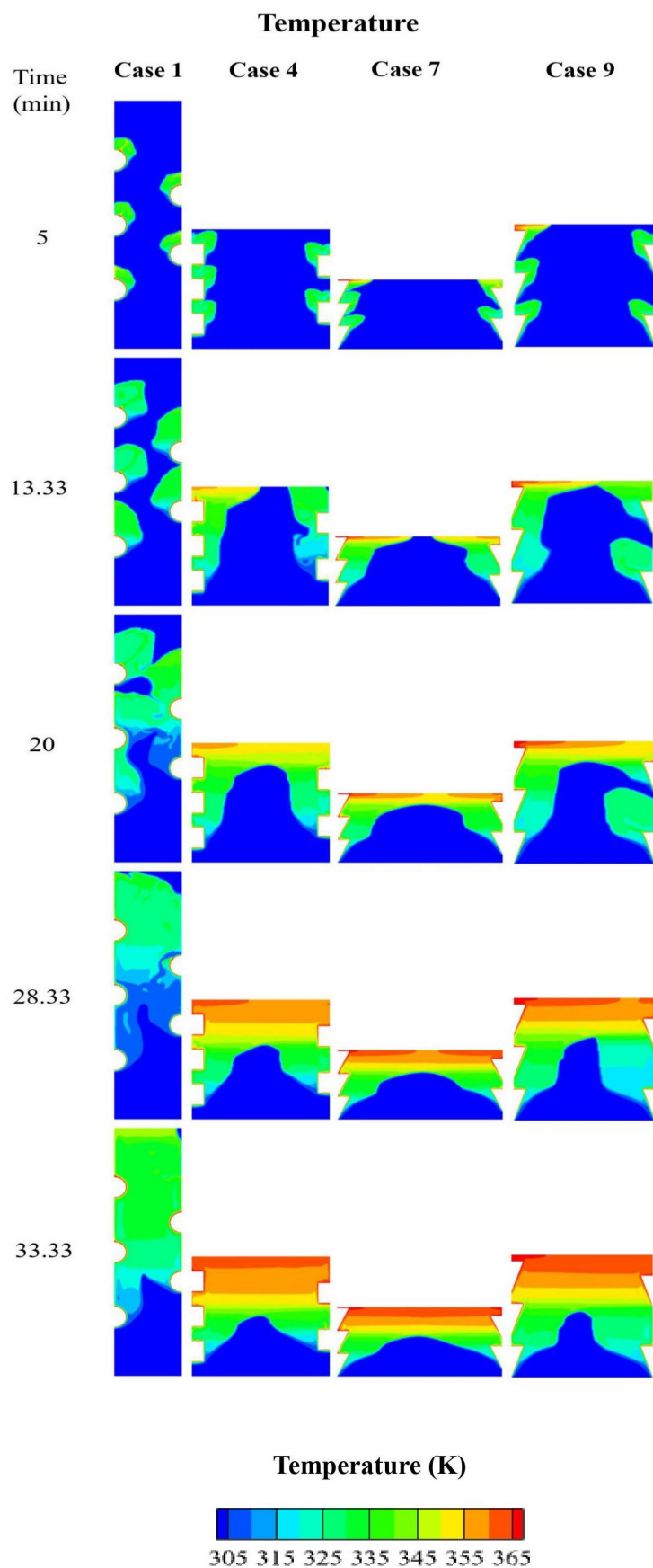FIGURE 5.2: Temporal variation of Melting fraction for Case 1, Case 4, Case 7, and optimum Case 9

Temperature

Temperature (K)

305 315 325 335 345 355 365

FIGURE 5.3: Temporal variation of Temperature for Case 1, Case 4, Case 7, and optimum Case 9

5.2 Melting Performance Enhancement

The primary objective of optimization is to improve the melting rate of the LHTES system. The efficiency of the system is determined numerically by calculating the enhancement ratio. Theoretically, the enhancement ratio Er can be calculated by the difference of melting fraction at different time steps of each case and base case (Case 1) of the L9 array table as illustrated in equation (5.1).

$$E_r = (\frac{\gamma_i - \gamma_1}{1.0}) \times 100\% \tag{5.1}$$

The rise in E_r value shows that the efficiency of the LHTES is improved in comparison to Case 1. The enhancement ratio for Case 4, Case 7, and Case 9 are presented in Figure 5.4 at different time steps in comparison to Case 1. Initially, the enhancement ratio remains the same for all the cases because at that time conduction effect is at its peak in the enclosure. After some time, convection heat transfer starts and at that time aspect ratio of the enclosure, the location of the tube, and the shape of the tube become a significant factor in enhancement. The highest value of enhancement ratio percentage for Case 9 is 7%, for Case 7 is 3% and for Case 4 is also 3%. After t = 10 mins, there is a sudden decline in the E_r percentage value for all cases. Case 4 and Case 7 E_r values become negative which shows that the melting fraction in Case 1 is higher than the other two respective cases. However, this impact is immediate, after t = 23.5 mins E_r value for all cases begins to rise once again. The next section goes into further information about this occurrence

5.3 Buoyant Flow Characteristics of Liquid PCM

During the phase change process, PCMs exhibit unique flow properties that have a significant impact on their performance characteristics. These properties are observed as the PCMs change state from solid and liquid. Having an indepth knowledge of these flow characteristics is necessary for optimizing the design and efficiency of the system. Figure 5.5 shows the velocity streamlines at different times
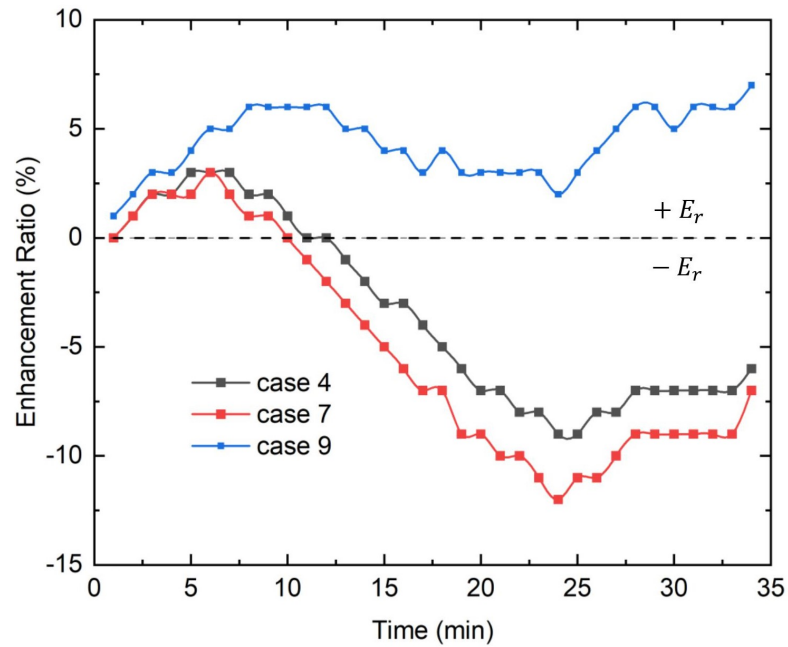
FIGURE 5.4: Temporal melting enhancement ratio for Case 4, Case 7, and optimum Case 9

for Case 1, Case 4, Case 7, and optimum Case 9 to help people understand. The interaction of vortices around the HTF tubes increases convection heat transfer. Streamlines for Case 1 at time t = 5 min boundary layer flow cause a small pair of vortices to form around the HTF tubes because of buoyancy driven flow. The HTF tubes at the bottom of the enclosure create vortices with very high temperatures, which speeds up the melting process in Case 9. The PCM liquid at the bottom of the container rises because of the difference in density and the buoyancy forces. When the temperature goes up, melted PCM forms a liquid coating around the HTF tubes that quickly grows. The formation of recirculating zones of liquid PCM around the HTF tubes slows down the convection effect and heat transfer at the bottom. At t = 5 min, the streamline plot for Case 4 shows a flow pattern of liquid phase change material that is similar to Case 1, except that, because the enclosure is wider, C-shaped vortices are formed in the middle and a pair of vortices form around the HTF tubes. The melting process of Case 1 creates recirculation zones at the upper part and around the symmetrical walls. These zones create significant disruption within the enclosure through their interaction with melting interfaces. In Case 4, the development of multiple vortices occurs around the HTF tubes, resulting in the formation of streamlines with a similar C-shaped pattern in the central region of the enclosure. Due to the temperature difference between the

liquid and solid PCM and the influence of buoyancy forces, circulation zones have emerged and are expanding as the melting process continues. During each step of the melting process, the velocity streamlines for Case 7 exhibit a consistent pattern as described for Case 1 and Case 4. Case 9 is the optimal configuration and has a comparable streamlined pattern. Over time, as the melting process intensifies, a significant amount of liquid phase change material develops around the HTF tubes and expands rapidly. The stream plots of the melting region in Case 9 exhibit higher density compared to other cases due to enhanced convection effects and heat transfer occurring between the solid and liquid sections.

5.4 Thermal Energy Storage Capacity

The LHTESU design involves essential parameters related to the rate of thermal energy storage. When the temperature rises, sensible energy is stored in the solid phase of phase change material, latent energy is stored during the phase transition process of phase change material, and sensible energy is stored again when the temperature rises in the liquid phase of phase change material. The cumulative specific energy of LHTES units for Case 1, Case 4, Case 7, and Case 9 are presented in Figure 5.6 at three different time intervals, namely t = 3.33 min, t = 16.33 min, and t = 32.61 min. At each time interval, Case 9 stores more heat energy than Case 1, Case 4, and Case 7 throughout. The peak specific thermal energy capacity attained by LHTESU for 75% melting is 58.76 kJ/kg, which is reached by Case 9 earlier than t = 32.61 mins. According to Case 1, the maximum specific thermal energy of 44.62 kJ/kg is stored at t = 32.61 mins which is 24% less than the optimum Case 9. Therefore, at earlier stages, conduction heat transfer dominates for a short time. However, after a short time, the buoyancy effect becomes significant, resulting in the initiation of natural convection due to variations in density. Natural convection enhances the rate of heat transfer between a liquid phase change material at a higher temperature and a solid PCM at a relatively lower temperature. Consequently, the liquid PCM releases heat, leading to an increase in the temperature difference among the heated surfaces of HTF tubes. This is the reason why the rate of specific energy storage decreases
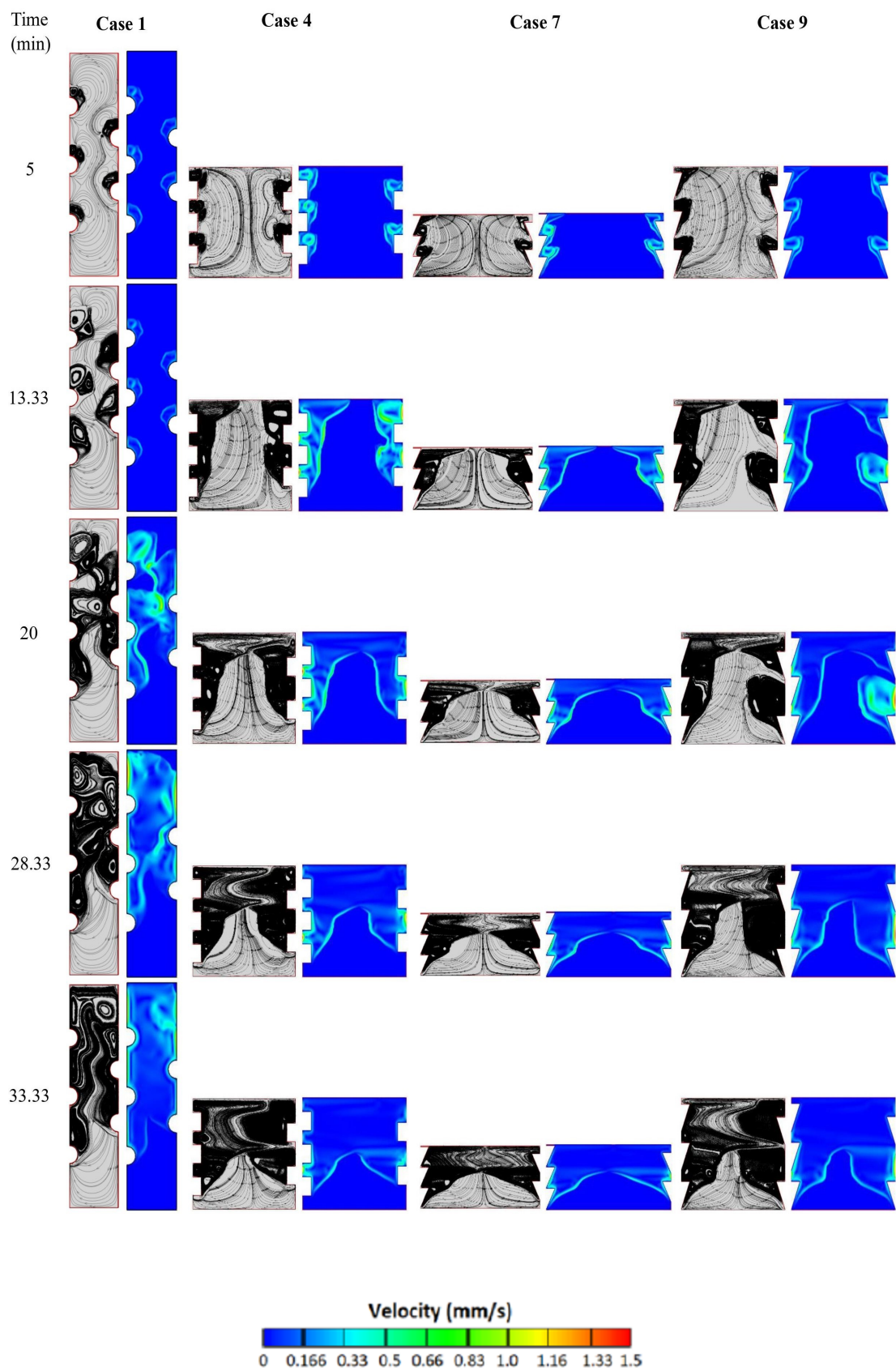
FIGURE 5.5: Streamlines and velocity contours for Case 1, Case 4, Case 7, and optimum Case 9

at a slower pace, and in the optimum configuration (Case 9), it nearly becomes constant due to the enhanced convection effect. The ability to store specific energy exhibited by Case 1 is comparatively lower than that of all the other cases. The rate of energy storage has a similar pattern to that observed in the enhancement ratio.
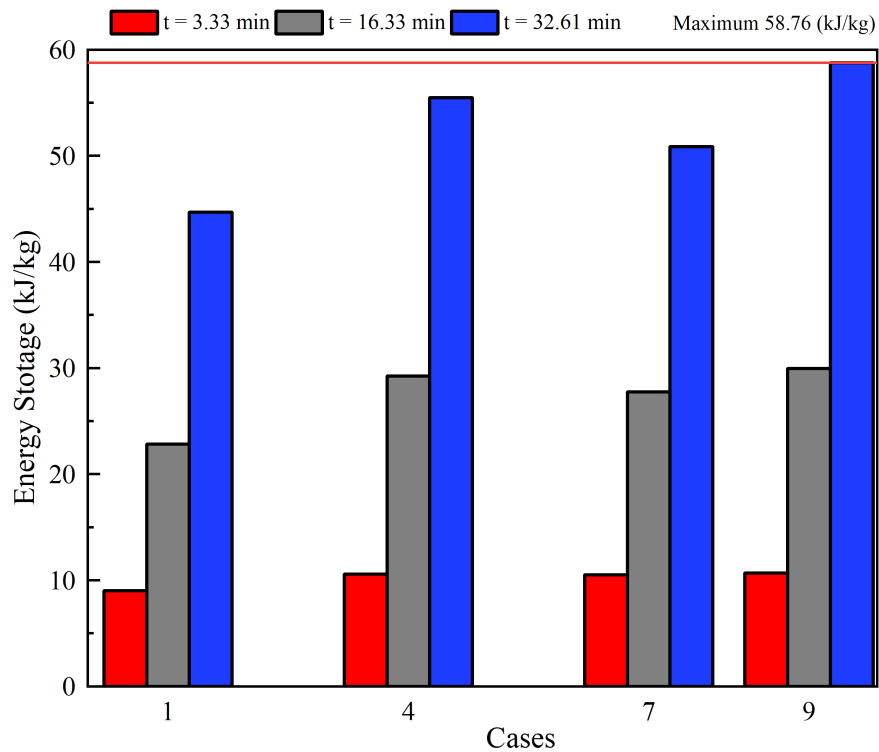
FIGURE 5.6: Specific energy storage comparison for Case 1, Case 4, Case 7, and optimum Case 9

5.5 Impact of HTF Temperature Variation on Melting

The HTF temperature directly affects the melting rate of phase change material in the LHTES unit. The Ste and Ra provided in equations (3.7, 3.8) can be associated with the variation in temperature of the tube. Table 5.1 presents the different Ste and Ra values corresponding to different HTF tube temperatures. Increasing the temperature of the HTF causes the increased variation in temperature between the hot tubes and the PCM, which in turn accelerates the melting rate of PCM. The temperature of the HTF in optimal Case 9 is defined by an isothermal boundary

condition applied to the inner surface of the HTF tubes. It ranges from 318 K to 368 K, with a 10 K interval. The Stefan number ranges from 0.0942 to 0.4290.

TABLE 5.1: Variation of HTF tube temperature of optimum Case 9

T_t (K)	Ste	Ra ($\times 10^6$)	m_t (mins)	F_o	$\overline{\text{Nu}}$
318	0.094	4.90	153.33	3.33	12.66
328	0.148	7.74	89.21	1.82	35.88
338	0.213	11.12	63.08	1.28	65.22
348	0.281	14.67	48.55	0.99	73.03
358	0.351	18.30	39.48	0.80	81.73
368	0.429	22.31	32.61	0.66	92.56

Figure 5.7 (a) illustrates the graph plot of the 75% melting time with different Stefan values, for optimal Case 9. As the Stefan number increases, the melting time of PCM decreases.The dropping trend follows an exponential pattern within the range of Stefan numbers between 0.09<Ste<0.42. However, after this range, the trend changes to a linear pattern. The reason for this is that the liquid phase change material develops an envelope around the heated surfaces, resulting in a reduction of conduction heat transfer. Nevertheless, the enhanced multi-tube configuration goes on in facilitating heat transfer and enhancing the melting process by inducing convective currents when conduction is hindered by the thick molten boundary layer of the phase change material. This phenomenon is illustrated in Figure 5.7 (b) where the relationship between the average Nusselt number and the Rayleigh number for different HTF temperatures.

A correlation equation 5.2 relates the 75% melting time (m_t) of phase change material (PCM) and the Stefan number (Ste). This equation is useful for estimating PCM melting durations in specific operating conditions and offers significant insight into the relationship among heat transfer mechanisms and phase change dynamics.

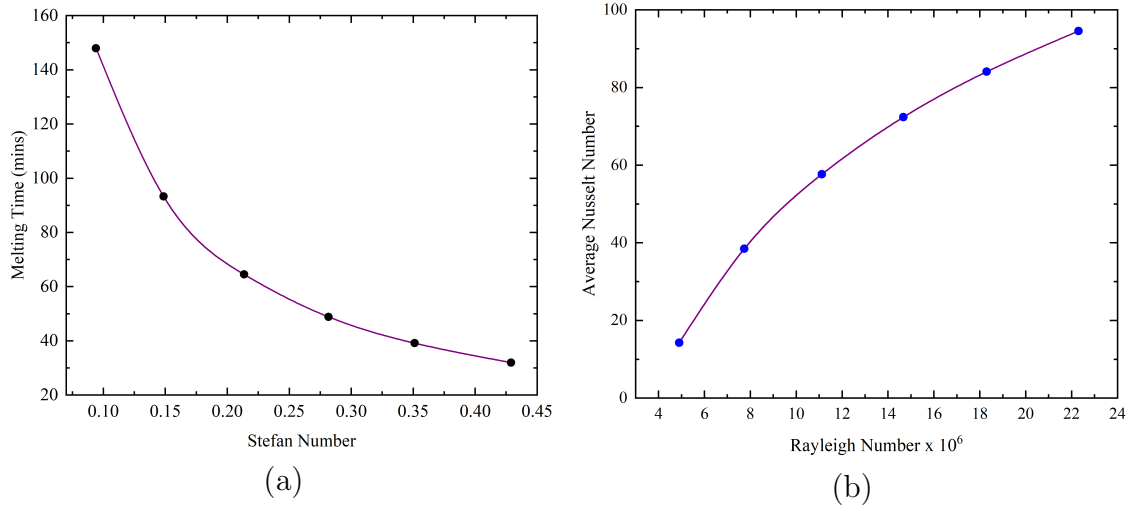$$m_t = A \times (Ste)^{-1.01} \tag{5.2}$$

FIGURE 5.7: Effects of HTF temperature variation on optimum Case 9 (a) 75% melting time is plotted against Stefan numbers, (b) Average Nusselt number is graphed against Rayleigh numbers.

Here, A = 13.6. The value of coefficient of determination (R^2) is 0.99 for this correlation equation which shows that the the correlation equation accurately captures the influence of the Stefan number on the melting time of the PCM, demonstrating a precise and reliable predictive capability. Table 5.2 shows the percentage error between melting time m_t and melting time correlation.

TABLE 5.2: Percentage error of Melting time (m_t) correlation

Ste	m_t (Num)	m_t (Corr)	Error (%)
0.094	153.33	147.95	3.63
0.148	89.21	93.28	4.35
0.214	63.08	64.53	2.25
0.282	48.55	48.84	0.57
0.351	39.48	39.13	0.90
0.429	32.61	31.97	2.00

The correlation equation 5.3 provides an interaction between the convective heat transfer coefficient, which is implicitly represented by the Nusselt number, and the governing flow parameters, which are represented by the Rayleigh number.

$$\overline{\text{Nu}} = B \times ln(Ra) - C \tag{5.3}$$

In equation 5.3 B = 53 and C = 70. The value of (R^2) is 0.98 for this correlation equation which indicates that around 98% of the variation in the average Nusselt number $\overline{\text{Nu}}$ can be explained by changes in the Rayleigh number (Ra). The correlation equation used is very reliable for estimating heat transfer rates in systems that exhibit natural convection. Table 5.3 illustrates the percentage error between average Nusselt number and average Nusselt number correlation.

TABLE 5.3: Percentage error of Average Nusselt Number correlation

$\mathbf{Ra} \times (10^6)$	$\overline{\text{Nu}}$ (Num)	$\overline{\text{Nu}}$ (Corr)	**Error (%)**
4.9	12.66	14.22	7.99
7.74	35.88	38.45	6.69
11.12	65.22	57.66	9.10
14.67	73.03	72.34	0.94
18.3	81.73	84.06	2.77
22.3	92.56	94.54	2.09

Chapter 6

Conclusion

Conclusion

Numerical analysis was utilized to optimize the 75% melting time of the LHTES unit. An extensive study was carried out on the convective heat transfer characteristics of the buoyant flow generated by the temperature change within the phase change material. The Taguchi method was used to optimize the physical design of the enclosure, focusing on the aspect ratio, tube location, and tube geometry. Utilizing average melting curves, average temperature distributions curves, melting contours, streamlines and velocity contours of Case 1, Case 4, Case 7 and Case 9 helps analyses phase change process within the LHTES system. The main results of this research are concisely summarized as follows:

1. Taguchi's design specifies that the enclosure's aspect ratio shall be 1, and each tube will possess a triangular geometry. Additionally specify that a few tubes need to be placed at the bottom zone (Z_{min}) of LHTESU.

2. Implementing Taguchi's design recommendations results in a 59% enhancement in the charging rate and a 24% improvement in the total specific energy capacity of the LHTES unit.

3. The primary factor influencing the design of the LHTES unit is the free convection flow during the meltdown process, as indicated by the melting

and temperature contours. We can see from the contours that a single large circulation flow within the enclosure is more efficient than numerous small and weak circulation flows.

4. The correlation between the melting time to reach 75% completion and the Nusselt numbers was analyzed by considering the Stefan number (Ste) and Rayleigh number (Ra) for the ideal configuration Case 9. The interactions precisely indicated the heat transfer and melting durations for various HTF temperatures.

Future Work and Recommendation

The outcomes of this study have created opportunities for further research in several aspects of improving thermal performance more effectively and efficiently. Regarding future work:

1. To overcome the low thermal conductivity of PCM, number of metallic and nonmetallic nanoparticles like Al_2O_3, CuO, SiO_2, TiO_2 can be used.

2. Fins can play vital role in increasing the heat transfer between HTF tubes and PCM. In future work we can enhance the melting rate by adding the fins in current LHTESU designs.

3. To improve the heat conduction within the LHTES system we can manipulate the geometry and angle of fins to increase the surface area and natural convection.

Bibliography

[1] L. G. SOCACIU, "Seasonal thermal energy storage concepts," *ACTA TECH-NICA NAPOCENSIS-Series: APPLIED MATHEMATICS, MECHANICS, and ENGINEERING*, vol. 55, no. 4, 2012.

[2] N. Belyakov, "Sustainable electricity management beyond generation," *Sustainable Power Generation*, 2019.

[3] F. U. Hasnain, "Numerical study to enhance the melting and solidification of phase change material using branched fins and nano-particles," Master's thesis, Capital University of Science and Technology, 2020.

[4] F. Jaeger, D. G. Beshore, F. M. Miller, and E. Gartner, "Applications of thermal energy storage in the cement industry," 1978.

[5] J. Soibam, "Numerical investigation of a phase change materials (pcm) heat exchanger-for small scale combustion appliances.," Master's thesis, NTNU, 2017.

[6] R. Qaiser, "Heat transfer enhancement of latent thermal energy storage system using multiple tubes and modified shell designs," Master's thesis, Capital University of Science and Technology, 2020.

[7] I. Sarbu and A. Dorca, "Review on heat transfer analysis in thermal energy storage using latent heat storage systems and phase change materials," *International journal of energy research*, vol. 43, no. 1, pp. 29–64, 2019.

[8] F. Agyenim, N. Hewitt, P. Eames, and M. Smyth, "A review of materials, heat transfer and phase change problem formulation for latent heat thermal

energy storage systems (lhtess)," *Renewable and sustainable energy reviews*, vol. 14, no. 2, pp. 615–628, 2010.

[9] M. Arıcı, F. Bilgin, S. Nižetić, and H. Karabay, "Pcm integrated to external building walls: An optimization study on maximum activation of latent heat," *Applied Thermal Engineering*, vol. 165, p. 114560, 2020.

[10] H. M. Ali and A. Arshad, "Experimental investigation of n-eicosane based circular pin-fin heat sinks for passive cooling of electronic devices," *International Journal of Heat and Mass Transfer*, vol. 112, pp. 649–661, 2017.

[11] Q. Fan, M. Liu, C. Zhang, W. Zhu, Y. Wang, P. Lin, F. Yan, L. Chen, H. J. Lezec, Y. Lu, *et al.*, "Independent amplitude control of arbitrary orthogonal states of polarization via dielectric metasurfaces," *Physical Review Letters*, vol. 125, no. 26, p. 267402, 2020.

[12] S. Bakhshipour, M. Valipour, and Y. Pahamli, "Parametric analysis of domestic refrigerators using pcm heat exchanger," *International journal of refrigeration*, vol. 83, pp. 1–13, 2017.

[13] M. A. Ezan, E. O. Doganay, F. E. Yavuz, and I. H. Tavman, "A numerical study on the usage of phase change material (pcm) to prolong compressor off period in a beverage cooler," *Energy conversion and management*, vol. 142, pp. 95–106, 2017.

[14] M. M. A. Khan, R. Saidur, and F. A. Al-Sulaiman, "A review for phase change materials (pcms) in solar absorption refrigeration systems," *Renewable and sustainable energy reviews*, vol. 76, pp. 105–137, 2017.

[15] S. Saha, A. R. M. Ruslan, A. Monjur Morshed, and M. Hasanuzzaman, "Global prospects and challenges of latent heat thermal energy storage: A review," *Clean Technologies and Environmental Policy*, vol. 23, pp. 531–559, 2021.

[16] S. Seddegh, X. Wang, and A. D. Henderson, "A comparative study of thermal behaviour of a horizontal and vertical shell-and-tube energy storage using phase change materials," *Applied Thermal Engineering*, vol. 93, pp. 348–358, 2016.

[17] İ. G. Demirkıran and E. Cetkin, "Computation time reduction of pcm melting process by changing modeling parameters," *Numerical Heat Transfer, Part A: Applications*, vol. 83, no. 1, pp. 50–67, 2022.

[18] R. Hamid and Z. Mehrdoost, "Thermal performance enhancement of multiple tubes latent heat thermal energy storage system using sinusoidal wavy fins and tubes geometry modification," *Applied Thermal Engineering*, p. 122750, 2024.

[19] Y. Li, G. Huang, T. Xu, X. Liu, and H. Wu, "Optimal design of pcm thermal storage tank and its application for winter available open-air swimming pool," *Applied Energy*, vol. 209, pp. 224–235, 2018.

[20] L. A. Khan and M. M. Khan, "Role of orientation of fins in performance enhancement of a latent thermal energy storage unit," *Applied Thermal Engineering*, vol. 175, p. 115408, 2020.

[21] A. A. Al-Abidi, S. B. Mat, K. Sopian, M. Sulaiman, C. Lim, and A. Th, "Review of thermal energy storage for air conditioning systems," *Renewable and Sustainable energy reviews*, vol. 16, no. 8, pp. 5802–5819, 2012.

[22] Q. Ren, P. Guo, and J. Zhu, "Thermal management of electronic devices using pin-fin based cascade microencapsulated pcm/expanded graphite composite," *International Journal of Heat and Mass Transfer*, vol. 149, p. 119199, 2020.

[23] H. Soltani, M. Soltani, H. Karimi, and J. Nathwani, "Optimization of shell and tube thermal energy storage unit based on the effects of adding fins, nanoparticles and rotational mechanism," *Journal of Cleaner Production*, vol. 331, p. 129922, 2022.

[24] M. A. Amidu, M. Ali, A. K. Alkaabi, and Y. Addad, "A critical assessment of nanoparticles enhanced phase change materials (nepcms) for latent heat energy storage applications," *Scientific Reports*, vol. 13, no. 1, p. 7829, 2023.

[25] C. Yang, Y. Xu, X. Cai, and Z.-J. Zheng, "Melting behavior of the latent heat thermal energy storage unit with fins and graded metal foam," *Applied Thermal Engineering*, vol. 198, p. 117462, 2021.

[26] J. Kong, H. Zuo, K. Zeng, Y. Lu, H. Xu, X. Zhang, H. Yang, and H. Chen, "Investigation of optimization methods for metal foam with two-dimensional porosity gradient in shell-and-tube latent heat storage," *Journal of Energy Storage*, vol. 63, p. 107004, 2023.

[27] F. Agyenim, P. Eames, and M. Smyth, "Heat transfer enhancement in medium temperature thermal energy storage system using a multitube heat transfer array," *Renewable energy*, vol. 35, no. 1, pp. 198–207, 2010.

[28] G. S. Sodhi, K. Vigneshwaran, A. K. Jaiswal, and P. Muthukumar, "Assessment of heat transfer characteristics of a latent heat thermal energy storage system: multi tube design," *Energy procedia*, vol. 158, pp. 4677–4683, 2019.

[29] J. Giro-Paloma, M. Martínez, L. F. Cabeza, and A. I. Fernández, "Types, methods, techniques, and applications for microencapsulated phase change materials (mpcm): A review," *Renewable and Sustainable Energy Reviews*, vol. 53, pp. 1059–1075, 2016.

[30] M. Hawlader, M. Uddin, and M. M. Khin, "Microencapsulated pcm thermal-energy storage system," *Applied energy*, vol. 74, no. 1-2, pp. 195–202, 2003.

[31] M. Al-Maghalseh and K. Mahkamov, "Methods of heat transfer intensification in pcm thermal storage systems," *Renewable and Sustainable Energy Reviews*, vol. 92, pp. 62–94, 2018.

[32] M. K. Rathod and J. Banerjee, "Thermal performance enhancement of shell and tube latent heat storage unit using longitudinal fins," *Applied Thermal Engineering*, vol. 75, pp. 1084–1092, 2015.

[33] P. H. Biwole, D. Groulx, F. Souayfane, and T. Chiu, "Influence of fin size and distribution on solid-liquid phase change in a rectangular enclosure," *International Journal of Thermal Sciences*, vol. 124, pp. 433–446, 2018.

[34] L. Pu, S. Zhang, L. Xu, and Y. Li, "Thermal performance optimization and evaluation of a radial finned shell-and-tube latent heat thermal energy storage unit," *Applied Thermal Engineering*, vol. 166, p. 114753, 2020.

[35] J. M. Mahdi, S. Lohrasbi, and E. C. Nsofor, "Hybrid heat transfer enhancement for latent-heat thermal energy storage systems: A review," *International Journal of Heat and Mass Transfer*, vol. 137, pp. 630–649, 2019.

[36] M. Yamaha and S. Misaki, "The evaluation of peak shaving by a thermal storage system using phase-change materials in air distribution systems," *Hvac&R Research*, vol. 12, no. S3, pp. 861–869, 2006.

[37] P. Dolado, A. Lazaro, J. M. Marin, and B. Zalba, "Characterization of melting and solidification in a real-scale pcm–air heat exchanger: Experimental results and empirical model," *Renewable Energy*, vol. 36, no. 11, pp. 2906–2917, 2011.

[38] A. Waqas and S. Kumar, "Phase change material (pcm)-based solar air heating system for residential space heating in winter," *International journal of green energy*, vol. 10, no. 4, pp. 402–426, 2013.

[39] F. Li, X. Huang, Y. Li, L. Lu, X. Meng, X. Yang, and B. Sundén, "Application and analysis of flip mechanism in the melting process of a triplex-tube latent heat energy storage unit," *Energy Reports*, vol. 9, pp. 3989–4004, 2023.

[40] J. Shen, P. Neveu, S. Shu, and Q. Falcoz, "Geometry optimization of a latent heat thermal energy storage unit using rt27," in *2016 5th International Conference on Environment, Materials, Chemistry and Power Electronics*, pp. 311–315, Atlantis Press, 2016.

[41] B. Huang, S. Yang, J. Wang, and P. D. Lund, "Optimizing the shape of pcm container to enhance the melting process," *Oxford Open Energy*, vol. 1, p. oiab006, 2022.

[42] N. B. Khedher, N. Biswas, H. Togun, H. I. Mohammed, J. M. Mahdi, R. K. Ibrahem, and P. Talebizadehsardari, "Geometry modification of a vertical shell-and-tube latent heat thermal energy storage system using a framed structure with different undulated shapes for the phase change material container during the melting process," *Journal of Energy Storage*, vol. 72, p. 108365, 2023.

[43] F. Fornarelli, M. Valenzano, B. Fortunato, S. Camporeale, M. Torresi, and P. Oresta, "Heat transfer enhancement induced by the geometry of a lhtes device," *Energy Procedia*, vol. 148, pp. 471–478, 2018.

[44] G. Mishra, A. Memon, A. K. Gupta, and N. Nirmalkar, "Computational study on effect of enclosure shapes on melting characteristics of phase change material around a heated cylinder," *Case Studies in Thermal Engineering*, vol. 34, p. 102032, 2022.

[45] H. Bai, "Research on optimization of tube structure of phase change heat storage device," in *Journal of Physics: Conference Series*, vol. 2166, p. 012040, IOP Publishing, 2022.

[46] R. Qaiser, M. M. Khan, H. F. Ahmed, F. K. Malik, M. Irfan, and I. U. Ahad, "Performance enhancement of latent energy storage system using effective designs of tubes and shell," *Energy Reports*, vol. 8, pp. 3856–3872, 2022.

[47] M. A. Alnakeeb, M. A. A. Salam, and M. A. Hassab, "Numerical treatment of melting characteristics of angular oriented flat tube in a double tube latent heat energy storage unit," *Case Studies in Thermal Engineering*, vol. 30, p. 101751, 2022.

[48] M. Ghalambaz, S. Mehryan, A. Hajjar, M. Y. A. Shdaifat, O. Younis, P. Talebizadehsardari, and W. Yaïci, "Thermal charging optimization of a wavy-shaped nano-enhanced thermal storage unit," *Molecules*, vol. 26, no. 5, p. 1496, 2021.

[49] Z.-J. Zheng, Y. Xu, and M.-J. Li, "Eccentricity optimization of a horizontal shell-and-tube latent-heat thermal energy storage unit based on melting and melting-solidifying performance," *Applied Energy*, vol. 220, pp. 447–454, 2018.

[50] A. Yadav, S. Samir, M. Arıcı, *et al.*, "A comprehensive study on melting enhancement by changing tube arrangement in a multi-tube latent heat thermal energy storage system," *Journal of Energy Storage*, vol. 55, p. 105517, 2022.

[51] M. Y. Yazıcı, M. Avcı, O. Aydın, and M. Akgun, "Effect of eccentricity on melting behavior of paraffin in a horizontal tube-in-shell storage unit: An experimental study," *Solar Energy*, vol. 101, pp. 291–298, 2014.

[52] M. Esapour, M. Hosseini, A. Ranjbar, and R. Bahrampoury, "Numerical study on geometrical specifications and operational parameters of multi-tube heat storage systems," *Applied Thermal Engineering*, vol. 109, pp. 351–363, 2016.

[53] A. Yadav, S. Samir, M. Arıcı, *et al.*, "Performance assessment of multi-tube inline and staggered array based latent heat storage system," *Journal of Energy Storage*, vol. 68, p. 107770, 2023.

[54] T. ur Rehman and H. M. Ali, "Experimental study on the thermal behavior of rt-35hc paraffin within copper and iron-nickel open cell foams: Energy storage for thermal management of electronics," *International Journal of Heat and Mass Transfer*, vol. 146, p. 118852, 2020.

[55] J. Vogel, J. Felbinger, and M. Johnson, "Natural convection in high temperature flat plate latent heat thermal energy storage systems," *Applied Energy*, vol. 184, pp. 184–196, 2016.

[56] A. Brent, V. R. Voller, and K. Reid, "Enthalpy-porosity technique for modeling convection-diffusion phase change: application to the melting of a pure metal," *Numerical Heat Transfer, Part A Applications*, vol. 13, no. 3, pp. 297–318, 1988.

[57] M. Kazemi, M. Hosseini, A. Ranjbar, and R. Bahrampoury, "Improvement of longitudinal fins configuration in latent heat storage systems," *Renewable Energy*, vol. 116, pp. 447–457, 2018.

[58] A. S. Soliman, A. A. Sultan, and M. A. Sultan, "Effect of mushy zone parameter on phase change behavior of different configurations storage unit: Numerical simulation and experimental validation," *Sustainability*, vol. 14, no. 21, p. 14540, 2022.

[59] T. Bouzennada, F. Mechighel, A. Filali, K. Ghachem, and L. Kolsi, "Numerical investigation of heat transfer and melting process in a pcm capsule: Effects of inner tube position and stefan number," *Case Studies in Thermal Engineering*, vol. 27, p. 101306, 2021.

[60] A. Pizzolato, A. Sharma, K. Maute, A. Sciacovelli, and V. Verda, "Topology optimization for heat transfer enhancement in latent heat thermal energy storage," *International Journal of Heat and Mass Transfer*, vol. 113, pp. 875–888, 2017.

[61] M. S. Shafiq, M. M. Khan, and M. Irfan, "Performance enhancement of double-wall-heated rectangular latent thermal energy storage unit through effective design of fins," *Case Studies in Thermal Engineering*, vol. 27, p. 101339, 2021.

[62] M. Ghalambaz, H. I. Mohammed, A. Naghizadeh, M. S. Islam, O. Younis, J. M. Mahdi, I. S. Chatroudi, and P. Talebizadehsardari, "Optimum placement of heating tubes in a multi-tube latent heat thermal energy storage," *Materials*, vol. 14, no. 5, p. 1232, 2021.